Cell Reports

Resource

Dynamic Transcriptome-Proteome Correlation Networks Reveal Human Myeloid Differentiation and Neutrophil-Specific Programming

Graphical Abstract

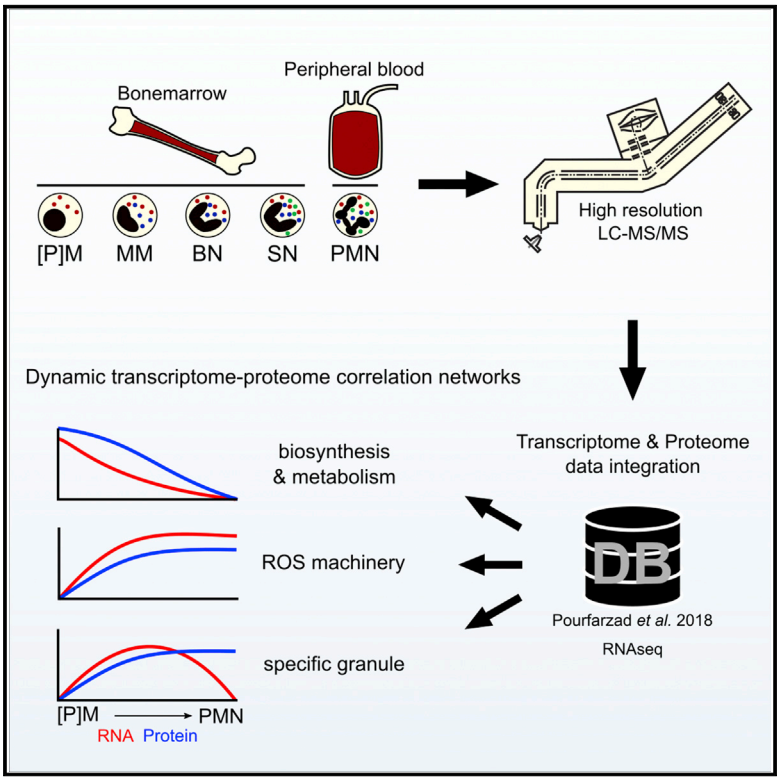

Highlights

- Dissection of transcriptome-proteome networks underlying neutrophil differentiation
- Distinct patterns of RNA-protein kinetics correlate with biological processes
- Discordant dynamics allows for functional annotation of granule proteins
- Anabolic collapse paradoxically coincides with gain in neutrophil function

Authors

Arie J. Hoogendijk, Farzin Pourfarzad, Cathelijn E.M. Aarts, ..., Alexander B. Meijer, Maartje van den Biggelaar, Taco W. Kuijpers

Correspondence

t.w.kuijpers@amsterdamumc.nl

In Brief

Human neutrophils form the largest pool of innate immune cells. Using mass spectrometry-based quantitative proteomics combined with transcriptomics, Hoogendijk et al. report on the dynamic changes of five developmental stages, unveiling highly dynamic RNA and protein kinetics that can be linked to functional maturation of end-stage blood neutrophils.

Hoogendijk et al., 2019, Cell Reports *29*, 2505–2519
November 19, 2019
https://doi.org/10.1016/j.celrep.2019.10.082

CellPress

Cell Reports
Resource

Dynamic Transcriptome-Proteome Correlation Networks Reveal Human Myeloid Differentiation and Neutrophil-Specific Programming

Arie J. Hoogendijk,[1] Farzin Pourfarzad,[2] Cathelijn E.M. Aarts,[2] Anton T.J. Tool,[2] Ida H. Hiemstra,[2] Luigi Grassi,[3] Mattia Frontini,[4,5] Alexander B. Meijer,[1,6] Maartje van den Biggelaar,[1,8] and Taco W. Kuijpers[2,7,8,9,*]
[1]Department of Molecular and Cellular Hemostasis, Sanquin Research, Amsterdam, the Netherlands
[2]Department of Blood Cell Research, Sanquin Research, Amsterdam University Medical Center (AUMC), University of Amsterdam, Amsterdam, the Netherlands
[3]Department of Haematology, University of Cambridge, Cambridge CB2 0PT, UK
[4]National Health Service Blood and Transplant, Cambridge Biomedical Campus, Cambridge CB2 0PT, UK
[5]British Heart Foundation Centre of Excellence, Cambridge Biomedical Campus, Long Road, Cambridge CB2 0QQ, UK
[6]Utrecht Institute for Pharmaceutical Sciences, Utrecht University, Utrecht, the Netherlands
[7]Department of Paediatric Immunology and Infectious Diseases, Emma Children's Hospital, AUMC, University of Amsterdam, Amsterdam, the Netherlands
[8]These authors contributed equally
[9]Lead Contact
*Correspondence: t.w.kuijpers@amsterdamumc.nl
https://doi.org/10.1016/j.celrep.2019.10.082

SUMMARY

Human neutrophilic granulocytes form the largest pool of innate immune cells for host defense against bacterial and fungal pathogens. The dynamic changes that accompany the metamorphosis from a proliferating myeloid progenitor cell in the bone marrow into a mature non-dividing polymorphonuclear blood cell have remained poorly defined. Using mass spectrometry-based quantitative proteomics combined with transcriptomic data, we report on the dynamic changes of five developmental stages in the bone marrow and blood. Integration of transcriptomes and proteome unveils highly dynamic and differential interactions between RNA and protein kinetics during human neutrophil development, which can be linked to functional maturation of typical end-stage blood neutrophil killing activities.

INTRODUCTION

Neutrophils form a first line of host defense against bacterial and fungal infections (Borregaard, 2010). In humans, these cells comprise 50%–70% of all blood-circulating leukocytes and can enter various tissues by extravasation from the blood circulation (Heifets, 1982). Neutrophils can perform an impressive array of killing activities to eliminate pathogens, which include phagocytosis, reactive oxygen species generation via the phagocyte NADPH oxidase, release of antimicrobial and cytotoxic compounds pre-stored in their intracellular granules, neutrophil extracellular trap (NET) formation, and secretion of chemokines and cytokines (Häger et al., 2010; Kolaczkowska and Kubes, 2013; Papayannopoulos and Zychlinsky, 2009).

The lifespan of circulating neutrophils is considered to be short (Lahoz-Beneytez et al., 2016; Pillay et al., 2010; Dancey et al., 1976). When released from the bone marrow, neutrophils circulate for some hours and then leave the bloodstream and enter the tissues for local defense at a constant rate of cellular turnover—unless they are directly attracted to a focal site of infection, where they can become activated by growth factors or inflammatory cytokines and may survive several days (Maianski et al., 2002, 2004; Moulding et al., 1998).

To accommodate the massive daily production of circulating non-dividing neutrophils, bone marrow progenitor cells need to proliferate extensively and commit to the myeloid lineage. During differentiation, neutrophil progenitor cells undergo impressively large changes, losing their proliferative capacity while obtaining the typical multi-lobulated nuclear morphology and killing activities that are required for exerting their crucial role in host defense. We hypothesize that this metamorphosis of myeloid progenitors into neutrophils is a well-balanced act between acquiring toxic protein machinery and avoiding any potential spill and damage to the bone marrow niche. However, despite the well-known morphological characterization of these stages, the differentiation pathways that regulate the kinetics of transcriptional and translational activity during human neutrophil maturation are poorly defined.

The current study reports on neutrophil development and function by proteomics using quantitative high-resolution mass spectrometry (MS) and integrates this with synchronized transcriptomic data to characterize these human phagocytes. We observed large decreases in metabolic and biosynthesis potential and, in parallel to this, the acquisition of essential neutrophil effector functions. In addition, we highlight the value of proteomics, because RNA levels were not indicative of protein abundancies. We also show that integration of multi-omic approaches enables greater understanding of the processes underlying neutrophil maturation, which include strong decreases

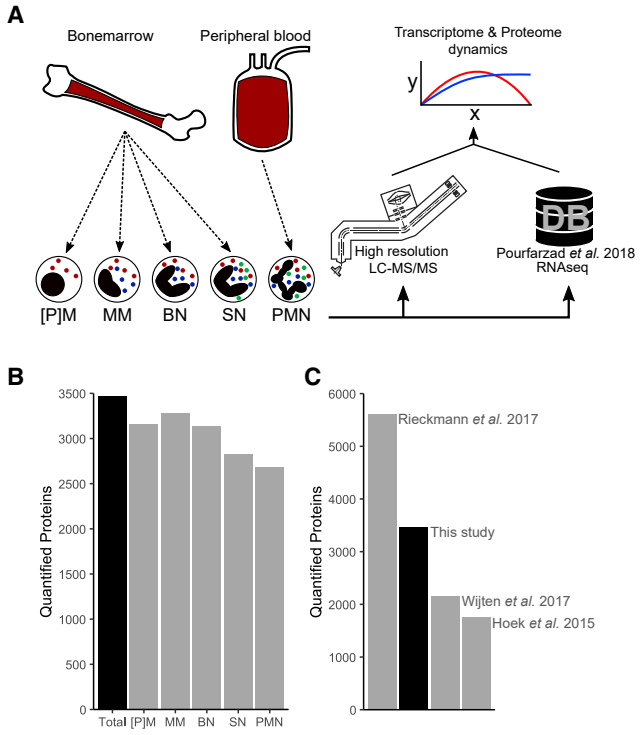

Figure 1. Dynamic Transcriptome-Proteome Correlation Networks in Neutrophil Differentiation

(A) Schematic of experimental setup and analysis. [P]Ms, MMs, SNs, and BNs from human bone marrow and PMNs from peripheral blood were isolated by flow cytometry and gradient centrifugation, respectively; analyzed by liquid chromatography-tandem mass spectrometry (LC-MS/MS); and integrated with RNA-seq data previously obtained from the same subsets.

(B) Number of quantified proteins for each of the obtained differentiation stages.

(C) Comparison of the number of quantified proteins in the present study with recent literature.

[P]Ms, (pro)myelocytes; MMs, metamyelocytes; BNs, band neutrophils; SNs, neutrophils with segmented nuclei; PMNs, blood-derived neutrophils. See also Table S1.

in metabolism and biosynthesis and the advent of, e.g., chemotaxis potential and granule content sorting.

Altogether, this study highlights critical aspects of the rapid transformation from a dividing progenitor into an end-stage kamikaze cell loaded with various toxic mechanisms to counter infections.

RESULTS

Integrated Transcriptomics and Proteomics of Neutrophil Development

To study human granulopoiesis *in vivo*, we dissected changes at the proteome level during neutrophil differentiation in the bone marrow and extravasation from the bone marrow into the blood (Figure 1A). We performed high-resolution mass spectrometry on fluorescence-activated cell sorted (FACS) myeloid progenitor cells derived from bone marrow—i.e., (pro)myelocytes ([P]Ms), metamyelocytes (MMs), immature neutrophils with a band-formed nucleus (BN), and mature neutrophils with segmented nuclei (SNs)—and on circulating neutrophils derived from blood (PMNs) (Figure S1A). MS data were analyzed with the MaxQuant computational platform (Cox and Mann, 2008). We combined our proteomic data with deep sequencing data on the same subsets (Grassi et al., 2018) to study whether and how transcriptomic changes lead to correlated proteome changes during granulopoiesis. We identified more than 65,000 peptides from more than 5,200 proteins. Of these, 3471 proteins were quantified in at least 3 samples in one of the subsets (Figure 1B; Table S1). Compared with previously published studies on the neutrophil proteome, our dataset ranks second in total quantified proteins (Figure 1C), behind an elegant dataset by Rieckmann et al. (2017). Although quantifying more proteins, this previous dataset used match between run in a set of many diverse cell types, which resulted in partial contamination of the neutrophil dataset with non-neutrophil proteins (e.g., CD8 and CD4). Unlike published neutrophil proteome studies, we obtained a set of primary differentiating neutrophil subsets, enabling investigation of human neutrophil ontology.

Extensive Proteomic Regulation during Neutrophil Differentiation and Extravasation

Principal-component analysis (based on label-free quantification [LFQ] values) clearly separated the myeloid differentiation stages with the exception of SNs and PMNs, demonstrating the robustness and reproducibility of the MS approach (Figure 2A). The [P]M proteome differed the most from the other four subsets, while the adjacency of SNs and PMNs indicated that the differences at the protein level between the final stage of SNs in the bone marrow (also known as the so-called bone marrow reserve pool of neutrophils) and blood-circulating PMNs are small. Pearson correlation coefficient of the label-free quantification (LFQ) values were calculated between the progenitor subsets (Figure 2B). This indicated a strong correlation of the proteome data between the progenitor subsets, with correlation coefficients dropping slightly between the first and the final differentiation stages. Next, LFQ values were transformed into absolute quantification values by means of the proteomic ruler methodology (Wiśniewski et al., 2014). During differentiation, the number of quantified proteins decreased slightly ($p < 0.001$, ANOVA), and we found that in mature neutrophils, 25% of the total protein copy numbers consisted of surprisingly low numbers of three highly abundant proteins (i.e., S100A8, S100A9, and HIST1H4A; Figure 2C). These absolute quantification values correspond well with the previous observation that the S100A8/9 complex constitutes ~40% of the neutrophil cytosolic protein content (Murthy et al., 1993).

By plotting the median estimated copy number against the cumulative protein copy number per subset, we observed that protein expression of all subsets showed a wide range of protein expression spanning more than seven orders of magnitude (Figure 2D). We overlaid proteins with, for neutrophils, the crucial function on this distribution, which revealed that most of these proteins increased in abundancy during differentiation (i.e., LTF, MMP8, MMP9, and NCF1), whereas elastase (ELANE) was already maximally present at the [P]M developmental stage. Of note, our observation of 5.3×10^7 [4.6×10^7–5.6×10^7]

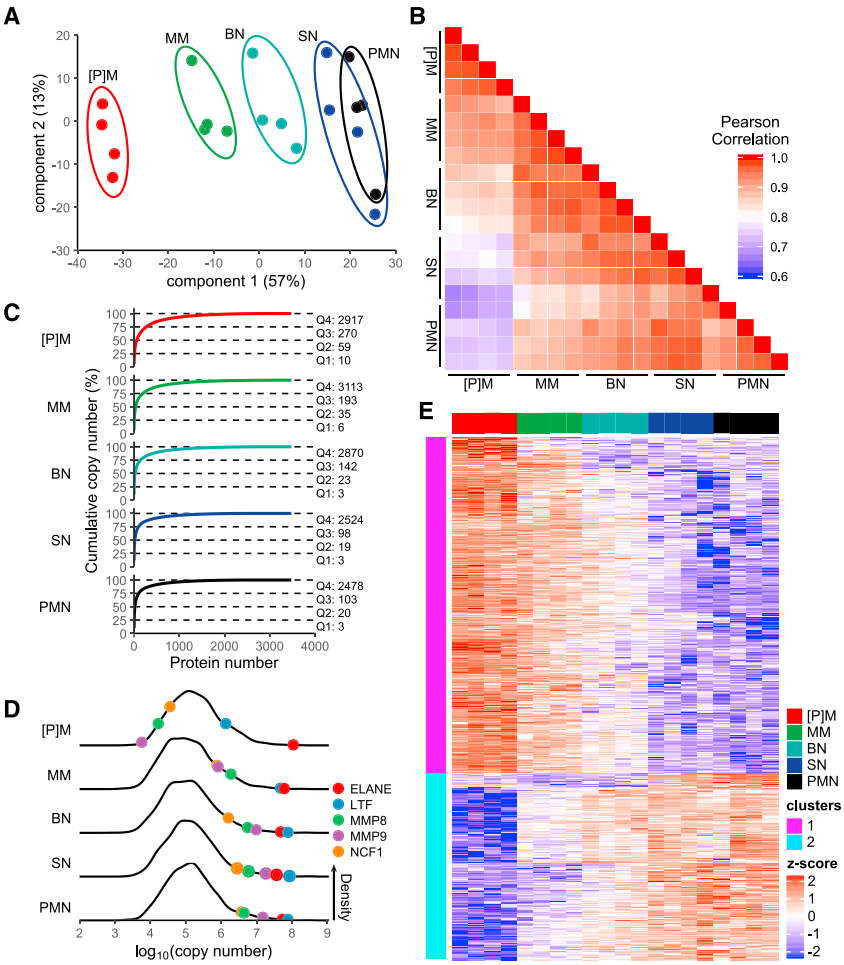

Figure 2. Proteome Profiles during Granulopoiesis

(A) Principal-component analysis of (pro)myelocyte ([P]M, red), metamyelocyte (MM, green), immature neutrophil with a band-formed nucleus (BN, teal), mature neutrophil with segmented nucleus (SN, blue), and circulating blood-derived neutrophil (PMN, black) proteomics data.

(B) Pearson correlation coefficients of neutrophil developmental stage proteomes. Color scale represents Pearson correlation coefficients.

(C) Cumulative distribution function plots depicting number of proteins per quartile of total for each developmental stage.

(D) Density plot of protein copy numbers, overlaid with hallmark neutrophil proteins.

(E) Heatmap of 874 differentially abundant proteins in neutrophil differentiation. Color scale represents *Z* scored LFQ values. K-mean clustering discriminates between decreased protein levels (cluster 1, magenta) and increased protein levels (cluster 2, cyan).

See also Table S1.

(median [IQR]) copy numbers of ELANE converts to 2.5 [2.2–2.6] pg/cell (median [IQR]), a value that is close to the 1.6 pg/cell previously estimated when measured by ELISA (Damiano et al., 1988).

The top 50 most abundant proteins in mature neutrophils included well-known neutrophil-derived granule proteins—(in order of protein copy number) LTF, CTSG, LYZ, CAMP, ELANE, MPO, AZU1, MMP9, and BPI—in addition to non-granule-derived proteins, such as histones, S100 proteins, and annexins (Table 1).

To identify protein levels that were significantly altered in neutrophil development, missing values were imputed with a normal distribution (width = 0.3; down shift = 1.8) and an ANOVA (false discovery rate [FDR] = 5% and S0 = 0.4) was performed. In total, 874 proteins were differentially abundant (Figure 2E; Table S1). Changes occurred in a gradual manner from [P]M to PMN, with either decreasing or increasing dynamics during differentiation. A larger number of proteins displayed a reduction rather than an increase in abundancy (562 versus 312 in clusters 1 and 2, respectively). This indicates that neutrophil differentiation is not only regulated by an overall gain of protein function but rather is the result of a balance between up- and downregulation of protein expression. Notably, we did not observe protein expression profiles that peaked or dipped in only one of the intermediate differentiation stages.

Kinetic Differences between RNA and Protein Expression during Differentiation

In recent years, the fundamental question of how the molecular mechanisms that govern mRNA transcription and protein translation are correlated has become a subject of discussion. Conflicting reports have been presented, ranging from observations that steady-state transcript levels can be used as proxies for protein levels (Edfors et al., 2016; Wilhelm et al., 2014); to observations of correlated global rewiring of RNA and protein expression, with most dynamic protein expression being transcription driven (Lindeboom et al., 2018); to pervasive discordance of mRNA and protein levels during differentiation and perturbation (Liu et al., 2016). To investigate whether and how changes in the transcriptome lead to proteomic changes during neutrophil development, we integrated our proteomic data with RNA sequencing (RNA-seq) results obtained on the same subsets (Grassi et al., 2018).

To identify overall correspondence between RNA and protein, we assessed the quantitative RNA levels (FPKM) of proteins that were quantified, identified but not quantified, or not detected. This analysis revealed that transcripts of proteins that were identified or quantified corresponded with higher median FPKM levels than other transcripts (Figure 3A; Figure S1C; ANOVA with Tukey post hoc test; $p < 0.001$). Genes that were expressed at FPKM levels below 1 were generally not quantified (Figure S1D; Fisher's exact tests; $p < 0.001$).

Table 1. Top 50 Expressed Proteins

	[P]M				MM				BN				SN				PMN			
Rank	Gene Name	Copy No.	%	Cum. %	Gene Name	Copy No.	%	Cum. %	Gene Name	Copy No.	%	Cum. %	Gene Name	Copy No.	%	Cum. %	Gene Name	Copy No.	%	Cum. %
1	HIST1H4A	1.7 E+8	5.4	5.4	S100A8	1.9 E+8	6.5	6.5	S100A8	3.0 E+8	10.4	10.4	S100A8	3.6 E+8	11.4	11.4	S100A9	3.1 E+8	9.8	9.8
2	CTSG	1.1 E+8	3.6	9.0	HIST1H4A	1.9 E+8	6.5	13.0	S100A9	2.3 E+8	7.9	18.3	S100A9	3.1 E+8	9.8	21.2	S100A8	3.0 E+8	9.6	19.4
3	ELANE	1.1 E+8	3.5	12.6	S100A9	1.8 E+8	6.0	19.0	HIST1H4A	1.8 E+8	6.3	24.6	HIST1H4A	2.0 E+8	6.3	27.4	HIST1H4A	1.9 E+8	6.1	25.5
4	MPO	7.6 E+7	2.4	15.0	LYZ	8.8 E+7	3.0	22.0	LTF	7.7 E+7	2.6	27.3	LYZ	8.6 E+7	2.7	30.2	COQ6	9.5 E+7	3.1	28.6
5	S100A8	6.3 E+7	2.0	17.0	CTSG	7.1 E+7	2.4	24.5	LYZ	7.6 E+7	2.6	29.9	LTF	8.4 E+7	2.7	32.9	LTF	7.7 E+7	2.5	31.1
6	LYZ	5.8 E+7	1.9	18.9	ELANE	6.1 E+7	2.1	26.5	CTSG	6.5 E+7	2.2	32.1	CTSG	6.4 E+7	2.0	34.9	CTSG	5.8 E+7	1.9	32.9
7	S100A9	5.3 E+7	1.7	20.6	LTF	4.8 E+7	1.6	28.2	PFN1	5.0 E+7	1.7	33.8	PFN1	5.8 E+7	1.9	36.8	S100A12	5.8 E+7	1.9	34.8
8	SERPINB1	4.9 E+7	1.6	22.1	PFN1	4.7 E+7	1.6	29.8	LCN2	4.9 E+7	1.7	35.5	LCN2	4.9 E+7	1.6	38.4	LYZ	5.7 E+7	1.8	36.6
9	AZU1	4.4 E+7	1.4	23.6	MPO	4.5 E+7	1.5	31.3	ELANE	4.8 E+7	1.6	37.1	CAMP	4.5 E+7	1.4	39.8	CAMP	5.5 E+7	1.8	38.4
10	DEFA1	3.8 E+7	1.2	24.8	LCN2	3.9 E+7	1.3	32.6	MPO	3.8 E+7	1.3	38.5	MPO	4.2 E+7	1.3	41.1	PFN1	5.5 E+7	1.8	40.2
11	P4HB	3.7 E+7	1.2	26.0	COQ6	3.5 E+7	1.2	33.8	CAMP	3.8 E+7	1.3	39.8	S100A12	3.7 E+7	1.2	42.3	ELANE	5.3 E+7	1.7	41.9
12	PFN1	3.3 E+7	1.1	27.0	RNASE3	3.3 E+7	1.1	35.0	SERPINB1	3.1 E+7	1.1	40.8	ELANE	3.7 E+7	1.2	43.5	LCN2	4.7 E+7	1.5	43.4
13	RNASE3	3.3 E+7	1.1	28.1	SERPINB1	3.1 E+7	1.1	36.1	ANXA1	2.9 E+7	1.0	41.8	COQ6	3.2 E+7	1.0	44.5	MPO	3.3 E+7	1.1	44.4
14	GSTP1	3.0 E+7	1.0	29.1	AZU1	2.9 E+7	1.0	37.0	ARHGDIB	2.5 E+7	0.8	42.7	SERPINB1	3.1 E+7	1.0	45.5	ANXA1	3.1 E+7	1.0	45.4
15	TMSB4X	2.4 E+7	0.8	29.9	ANXA1	2.8 E+7	1.0	38.0	S100A12	2.3 E+7	0.8	43.5	ANXA1	3.1 E+7	1.0	46.5	SERPINB1	3.0 E+7	1.0	46.4
16	PPIB	2.4 E+7	0.8	30.6	DEFA1	2.4 E+7	0.8	38.8	COQ6	2.3 E+7	0.8	44.3	S100A6	2.9 E+7	0.9	47.4	S100P	2.9 E+7	0.9	47.3
17	PRG2	2.4 E+7	0.8	31.4	TKT	2.2 E+7	0.7	39.5	TKT	2.2 E+7	0.8	45.1	LCP1	2.6 E+7	0.8	48.3	S100A6	2.8 E+7	0.9	48.2
18	TKT	2.3 E+7	0.7	32.1	TMSB4X	2.1 E+7	0.7	40.3	LCP1	2.2 E+7	0.8	45.8	ARHGDIB	2.5 E+7	0.8	49.0	S100A4	2.8 E+7	0.9	49.1
19	ARHGDIB	2.3 E+7	0.7	32.8	CAMP	2.0 E+7	0.7	41.0	AZU1	2.1 E+7	0.7	46.6	TMSB4X	2.5 E+7	0.8	49.8	AZU1	2.5 E+7	0.8	49.9

(*Continued on next page*)

Table 1. *Continued*

	[P]M				MM				BN				SN				PMN			
Rank	Gene Name	Copy No.	%	Cum. %	Gene Name	Copy No.	%	Cum. %	Gene Name	Copy No.	%	Cum. %	Gene Name	Copy No.	%	Cum. %	Gene Name	Copy No.	%	Cum. %
20	S100P	2.2 E+7	0.7	33.6	ARHGDIB	2.0 E+7	0.7	41.7	RNASE3	2.1 E+7	0.7	47.3	VIM	2.3 E+7	0.7	50.6	VIM	2.5 E+7	0.8	50.7
21	HIST1H1B	2.0 E+7	0.6	34.2	GSTP1	2.0 E+7	0.7	42.4	GCA	1.9 E+7	0.7	47.9	TKT	2.3 E+7	0.7	51.3	ARHGDIB	2.4 E+7	0.8	51.5
22	ANXA1	1.8 E+7	0.6	34.8	LDHA	1.9 E+7	0.6	43.0	LDHA	1.9 E+7	0.7	48.6	S100A11	2.3 E+7	0.7	52.0	LCP1	2.4 E+7	0.8	52.3
23	H2AFV	1.8 E+7	0.6	35.3	LCP1	1.8 E+7	0.6	43.6	HIST1H2BN	1.8 E+7	0.6	49.2	S100A4	2.1 E+7	0.7	52.7	TKT	2.2 E+7	0.7	53.0
24	RPLP2	1.8 E+7	0.6	35.9	P4HB	1.8 E+7	0.6	44.2	GSTP1	1.8 E+7	0.6	49.8	LDHA	2.0 E+7	0.6	53.3	HIST1H3A	2.1 E+7	0.7	53.7
25	CAT	1.8 E+7	0.6	36.5	GCA	1.7 E+7	0.6	44.8	PGK1	1.8 E+7	0.6	50.4	PGK1	2.0 E+7	0.6	54.0	GSTP1	2.1 E+7	0.7	54.4
26	LCP1	1.6 E+7	0.5	37.0	PGK1	1.7 E+7	0.6	45.4	HIST1H1B	1.7 E+7	0.6	51.0	AZU1	1.9 E+7	0.6	54.6	PGK1	2.0 E+7	0.6	55.0
27	RNASE2	1.6 E+7	0.5	37.5	PRDX5	1.6 E+7	0.6	45.9	VIM	1.6 E+7	0.6	51.6	MMP9	1.8 E+7	0.6	55.2	S100A11	2.0 E+7	0.6	55.6
28	PGK1	1.6 E+7	0.5	38.0	PRG2	1.6 E+7	0.5	46.5	MNDA	1.5 E+7	0.5	52.1	HIST1H1B	1.8 E+7	0.6	55.7	LDHA	1.9 E+7	0.6	56.3
29	EPX	1.5 E+7	0.5	38.5	S100P	1.6 E+7	0.5	47.0	P4HB	1.3 E+7	0.5	52.6	GSTP1	1.8 E+7	0.6	56.3	MNDA	1.9 E+7	0.6	56.9
30	HIST1H2BN	1.5 E+7	0.5	39.0	HIST1H3A	1.5 E+7	0.5	47.5	HIST1H3A	1.3 E+7	0.4	53.0	RNASE3	1.8 E+7	0.6	56.9	GCA	1.9 E+7	0.6	57.5
31	LDHA	1.5 E+7	0.5	39.5	HIST1H1B	1.5 E+7	0.5	48.0	S100A6	1.3 E+7	0.4	53.4	GCA	1.7 E+7	0.6	57.4	TXN	1.6 E+7	0.5	58.0
32	PRDX5	1.5 E+7	0.5	39.9	MNDA	1.4 E+7	0.5	48.5	PRDX5	1.2 E+7	0.4	53.9	MNDA	1.7 E+7	0.6	58.0	MMP9	1.5 E+7	0.5	58.4
33	TXN	1.5 E+7	0.5	40.4	HIST1H2BN	1.4 E+7	0.5	49.0	BPI	1.1 E+7	0.4	54.3	S100P	1.7 E+7	0.5	58.5	PGD	1.4 E+7	0.5	58.9
34	HIST1H3A	1.4 E+7	0.5	40.9	HIST2H3A	1.3 E+7	0.4	49.4	PGAM1	1.1 E+7	0.4	54.6	TXN	1.5 E+7	0.5	59.0	RNASE3	1.3 E+7	0.4	59.3
35	HSPA5	1.4 E+7	0.4	41.3	PGAM1	1.3 E+7	0.4	49.8	TPI1	1.1 E+7	0.4	55.0	PRDX5	1.4 E+7	0.4	59.5	ALDOA	1.3 E+7	0.4	59.7
36	ALDOA	1.3 E+7	0.4	41.7	BPI	1.3 E+7	0.4	50.3	ALDOA	1.1 E+7	0.4	55.4	HIST1H2BN	1.3 E+7	0.4	59.9	HIST1H1B	1.3 E+7	0.4	60.1
37	HIST2H3A	1.3 E+7	0.4	42.2	PPIB	1.2 E+7	0.4	50.7	GPI	1.1 E+7	0.4	55.8	TPI1	1.3 E+7	0.4	60.3	PGAM1	1.2 E+7	0.4	60.5
38	PPIA	1.3 E+7	0.4	42.6	H2AFV	1.2 E+7	0.4	51.1	CAT	1.1 E+7	0.4	56.1	PGAM1	1.3 E+7	0.4	60.7	HIST1H2BN	1.2 E+7	0.4	60.9

(*Continued on next page*)

Table 1. *Continued*

	[P]M				MM				BN				SN				PMN			
Rank	Gene Name	Copy No.	%	Cum. %	Gene Name	Copy No.	%	Cum. %	Gene Name	Copy No.	%	Cum. %	Gene Name	Copy No.	%	Cum. %	Gene Name	Copy No.	%	Cum. %
39	TPI1	1.3 E+7	0.4	43.0	RNASE2	1.2 E+7	0.4	51.5	PGD	1.1 E+7	0.4	56.5	PGD	1.2 E+7	0.4	61.1	HIST2H3A	1.2 E+7	0.4	61.3
40	GCA	1.2 E+7	0.4	43.4	TPI1	1.1 E+7	0.4	51.9	CALM1	1.0 E+7	0.3	56.8	HIST2H3A	1.2 E+7	0.4	61.5	PRDX5	1.1 E+7	0.4	61.7
41	PGAM1	1.2 E+7	0.4	43.8	CAT	1.1 E+7	0.4	52.3	YWHAZ	9.9 E+6	0.3	57.2	HIST1H3A	1.2 E+7	0.4	61.9	MYL12A	1.0 E+7	0.3	62.0
42	CALM1	1.1 E+7	0.4	44.1	CALM1	1.1 E+7	0.4	52.7	MMP9	9.8 E+6	0.3	57.5	CFL1	1.2 E+7	0.4	62.2	STOM	9.8 E+6	0.3	62.3
43	HSP90B1	1.0 E+7	0.3	44.5	VIM	1.1 E+7	0.4	53.0	TMSB4X	9.3 E+6	0.3	57.8	ALDOA	1.1 E+7	0.4	62.6	YWHAZ	9.8 E+6	0.3	62.6
44	PNP	9.8 E+6	0.3	44.8	GPI	1.1 E+7	0.4	53.4	TXN	9.3 E+6	0.3	58.1	YWHAZ	1.1 E+7	0.4	63.0	TPI1	9.5 E+6	0.3	62.9
45	MNDA	9.6 E+6	0.3	45.1	TXN	1.0 E+7	0.4	53.8	S100A11	9.2 E+6	0.3	58.5	CALM1	1.1 E+7	0.4	63.3	BPI	9.3 E+6	0.3	63.2
46	PDIA3	9.6 E+6	0.3	45.4	S100A11	1.0 E+7	0.3	54.1	CFL1	9.0 E+6	0.3	58.8	BPI	1.1 E+7	0.4	63.7	CAPZB	9.3 E+6	0.3	63.5
47	PGD	9.0 E+6	0.3	45.7	STOM	9.9 E+6	0.3	54.4	STOM	8.8 E+6	0.3	59.1	CAPZB	9.7 E+6	0.3	64.0	CALM1	9.3 E+6	0.3	63.8
48	ENO1	9.0 E+6	0.3	46.0	PGD	9.6 E+6	0.3	54.8	HIST2H3A	8.7 E+6	0.3	59.4	GPI	9.7 E+6	0.3	64.3	HMGB2	8.9 E+6	0.3	64.1
49	LDHB	9.0 E+6	0.3	46.3	EPX	9.4 E+6	0.3	55.1	HMGB2	8.6 E+6	0.3	59.7	CAT	9.6 E+6	0.3	64.6	ARPC2	8.7 E+6	0.3	64.4
50	GPI	8.9 E+6	0.3	46.6	ALDOA	9.4 E+6	0.3	55.4	CAPZB	8.5 E+6	0.3	60.0	STOM	9.3 E+6	0.3	64.9	MSN	8.6 E+6	0.3	64.7

Top 50 expressed proteins based on protein copy number, percentage of the total, and cumulative percentage (Cum. %). [P]M, (pro)myelocyte; MM, metamyelocyte; BN, band neutrophil; SN, neutrophil with segmented nucleus; PMN, blood-derived neutrophil.

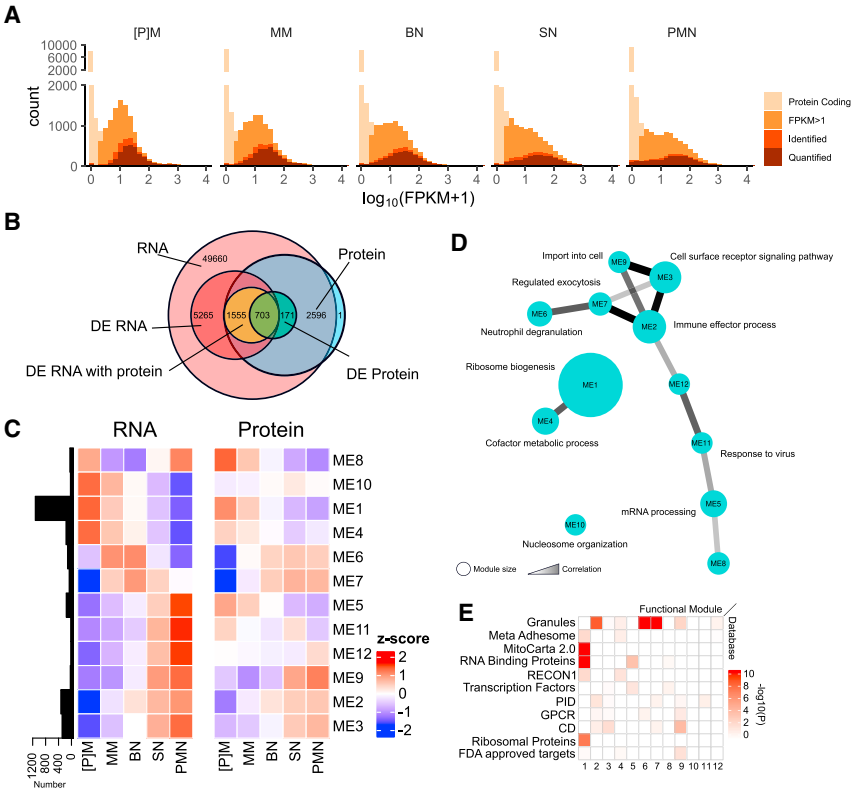

Figure 3. Transcriptome and Proteome Co-expression Network Analysis

(A) Histograms of the RNA expression range depicted as median $\log_{10}$(FPKM+1) values. Protein coding genes are shown in salmon, all protein coding genes with FPKM > 1 are shown in orange, proteins that are identified are shown in tawny, and proteins that are quantified are shown in brown.

(B) Venn diagram depicting overlap and distribution of expressed RNA, differentially expressed RNA (DE RNA), quantified proteins, and differentially expressed proteins (DE protein) during granulopoiesis.

(C) Transcript-protein pairs differentially expressed on either the RNA or the protein level were subjected to weighted gene cluster network analysis, resulting in 12 modules (MEs). Heatmap of 12 WGCNA modules, split over RNA and protein data. Bars on the left represent the number of transcript-protein pairs per modules. Bar plot depicts the number of transcript-protein pairs per module. Colors represent *Z* scored expression values.

(D) Neutrophil differentiation module network. Node circumference reflects module size, edge opacity represents Pearson correlation coefficients, and correlations > 0.6 are shown. Highly enriched GO terms are annotated to nodes.

(E) Heatmap of enrichment of manually annotated curated databases per functional module. Color intensity represents $-\log_{10}$(P).

See also Figures S1–S3 and S7 and Tables S1, S2, and S3.

Comparing the subsequent stages of differentiation, we observed a shift of quantified proteins to genes that are expressed at lower FPKM values (Figure 3A). Finally, at the end stage of differentiation, i.e., mature circulating neutrophils, a significant number of quantified proteins exhibited RNA levels of FPKM < 1 ($p < 0.001$; Figure S1E).

To elucidate transcript-protein dynamics, we performed unbiased clustering based on the correlation of protein and RNA expression patterns (Langfelder and Horvath, 2008). Using 2,429 transcript-protein pairs that were differentially expressed during neutrophil development in RNA, protein, or both datasets (Figure 3B), we performed weighted gene co-expression network analysis (WGCNA). This resulted in a network consisting of 12 modules (MEs) (Figure 3C), ranging in size from 23 to 1,119 transcript-protein pairs. Hub transcript-protein pairs were determined for each module, for which the top four of each are shown in Figure S2.

The transcriptome-proteome correlation network analyses revealed patterns of concordant decreases and increases in RNA and protein levels for >70% of the transcript-protein pairs (ME1–ME4). However, the remaining ~30% of transcript-protein pairs showed a varying degree of discordance between RNA and protein dynamics (ME5–ME12). The most prominent discordant pattern included subsets of proteins for which RNA expression dropped during differentiation while protein expression remained similar. This may be indicative of protein storage or sequestration in macromolecular protein complexes (ME6, ME7, and ME10). In contrast, we also observed discordant patterns in which RNA expression increases during differentiation but protein levels drop (ME5 and ME8) or remain stable (ME11 and ME12) (Table S1).

To retrieve the functional biological processes that accompany neutrophil development, we performed pathway analysis (Figure S3A;Table S2) and Gene Ontology (GO) enrichment analysis (Yu et al., 2012) (Table S3) and annotated highly significant terms to a Pearson correlation-based module network (Figure 3D). This revealed that modules with similar functions correlated well with one another. Both ME1 and ME4 described a decreased in cellular biosynthesis associated terms, whereas gain of neutrophil function terms clustered together (i.e., ME2, ME3, ME6, and ME7), such as "neutrophil degranulation" and "immune effector process."

In addition to GO enrichment, we selected curated databases of proteins function for manual enrichment of module functions (cluster of differentiation, GPCR, FDA-approved targets, transcription factors, and ribosomal proteins: Human Protein Atlas v.18.1 [Thul et al., 2017]; granule proteins [Rørvig et al., 2013]; meta-adhesome [Horton et al., 2015]; primary immunodeficiency genes [Picard et al., 2015]; RNA binding proteins [Gerstberger et al., 2014]; RECON1 [Duarte et al., 2007]; and MitoCarta 2.0 [Calvo et al., 2016]). In concordance with GO enrichment, ME1 enriched for biosynthesis, as well as mitochondrial and RNA binding annotations (Figure 3E). In further agreement with GO enrichment, granular protein annotations were enriched in modules describing increased protein abundancies and specifically in ME6 and ME7.

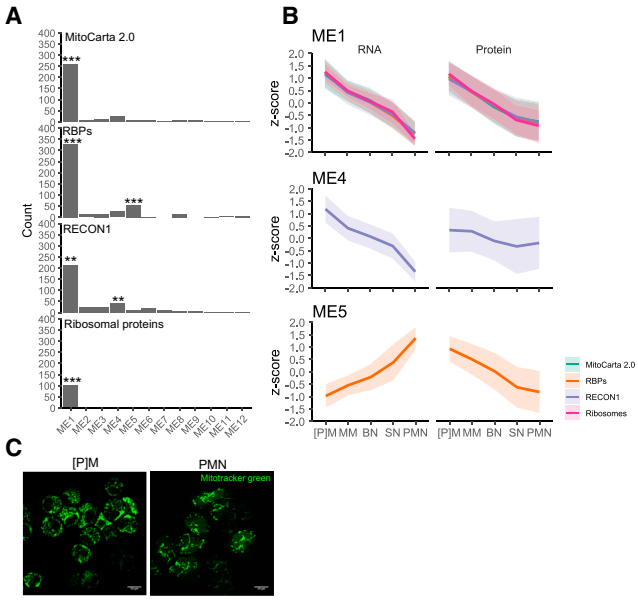

Figure 4. Collapse of Biosynthesis and Metabolic Potential

(A) Bar graphs showing module membership distribution of transcript-protein pairs for MitoCarta 2.0, RNA binding proteins (RBPs), RECON1, and ribosomal protein annotation.

(B) Line (mean) and ribbon (SD) plots showing dynamics of enriched transcript-protein pairs.

(C) Mitochondrial staining in (pro)myelocytes and blood-derived circulating neutrophils by means of MitoTracker Green. Representative images are shown.

Scale bars, 10 μm. $^{**}p < 0.01$, $^{***}p < 0.001$ as determined with Fisher's exact tests. Lines represent means; ribbons represent SDs. See also Figures S3 and S4 and Table S2.

General Decline in Mitochondrial, Metabolic, and Protein Synthesis Processes

GO enrichment and manually annotated database enrichment indicated a decline in anabolic processes. To further define the dynamics of these database annotations, we overlaid metabolic and protein production processes (i.e., MitoCarta 2.0, RNA binding proteins [RBPs], RECON1, and ribosomal protein annotation) onto the function modules (Figure 4A).

An intact mitochondrial function is essential for myeloid development, suggesting that the initial stages of granulopoiesis depend on ATP-dependent transcriptional processes (Szatmary et al., 2017). During maturation, the level of mitochondrial activity decreases and mature neutrophils only possess a limited number of mitochondria (Maianski et al., 2002, 2004; van Raam et al., 2006, 2008). Despite this limited number, mitochondria still play a central role in the regulation of neutrophil survival and programmed cell death (Maianski et al., 2004). In agreement with the observation that mitochondria no longer contribute to the energy status of circulating neutrophils, expression profiles of transcripts and proteins associated with processes related to ATP production in mitochondria, including oxidative phosphorylation and electron transport chain, were decreased (Figure S3A; Table S2).

Of the collection of 1,158 nuclear and mtDNA genes encoding proteins with strong support of mitochondrial localization (MitoCarta 2.0) (Calvo et al., 2016), 338 showed a significantly different expression profile (Figure 4A). In general, protein expression decreased during differentiation, and most corresponding transcript-protein pairs demonstrated the concomitant decrease of RNA and protein (ME1) (Figure 4B). This was accompanied by a change in mitochondrial morphology from round to a more tubular phenotype (Figure 4C). In agreement with our previous report on the functional inability of neutrophil mitochondria to generate ATP (van Raam et al., 2008), we observed that the proteins involved in oxidative phosphorylation (Figure S3B) and electron transport chain (complex I, II, III, IV, and V) (Figure S3C) showed steep decreases during myeloid differentiation.

To further study alterations in general cell metabolism, we performed enrichment analysis using the human metabolic reconstruction RECON1 database containing 1,496 metabolic proteins (Duarte et al., 2007). Of these, 369 were significantly up- or downregulated in our dataset (Figure 4A), with kinetics largely overlapping with the mitochondrial protein profiles (Figure 4B). Enzymes involved in regulation of the mitochondrial tricarboxylic acid (TCA) cycle (e.g., OGDH, SDHA, SUCLG2, IDH2, and ACO2) were all downregulated (Figure S3D). The TCA cycle consists of a series of reactions used by most cells to release stored energy through the oxidation of acetyl-CoA derived from carbohydrates, fatty acids, and proteins into carbon dioxide and chemical energy in the form of ATP. Indeed, neutrophils rely on glycolysis to generate ATP (van Raam et al., 2008), which matches our observations.

Another important class of proteins involved in regulating post-transcriptional mechanisms, including RNA processing (splicing, capping, and polyadenylation), transport, decay, localization, and translation, consists of RNA binding proteins (RBPs) (Hentze et al., 2018). Of 1,542 annotated RBPs (Gerstberger et al., 2014), 460 showed a significantly different profile (Figure 4A). Most RBPs displayed a reduction in RNA and protein levels (ME1), whereas a set of 54 RBPs were members of ME5, for which there is an increase in RNA levels combined with a decrease in protein abundancy (Figures 4A and 4B).

We also observed a decreased expression profile for ribosomal proteins (Figures 4A and 4B; Figures S3A and S4A), as well as DNA replication (Figure S4B; Table S2), which includes the mini-chromosome maintenance (MCM) complex of six proteins. The MCM complex controls DNA replication in eukaryotic cells that occurs once per cell cycle. All observed MCM complex members displayed decreased RNA and proteins levels during differentiation and were categorized in ME1 (Figure S4C).

Altogether, these results suggest an almost complete loss of regulation at the transcriptional and post-transcriptional level and a severely diminished metabolic potential during PMN development.

Gain of Strong Motile Capacity

Modules describing increased protein levels during neutrophil differentiation (ME2, ME3, ME6, ME7, and ME9) enriched for processes that are specific for neutrophil function (Figures 3C–3E; Figure S2). Notable enriched GO terms included G-protein coupled receptor signaling pathways (Table S3). Of the 753 annotated GPCRs (Human Protein Atlas v.18.1; Thul et al., 2017), 13 GPCRs were present in our data (Table S1). Flow cytometry

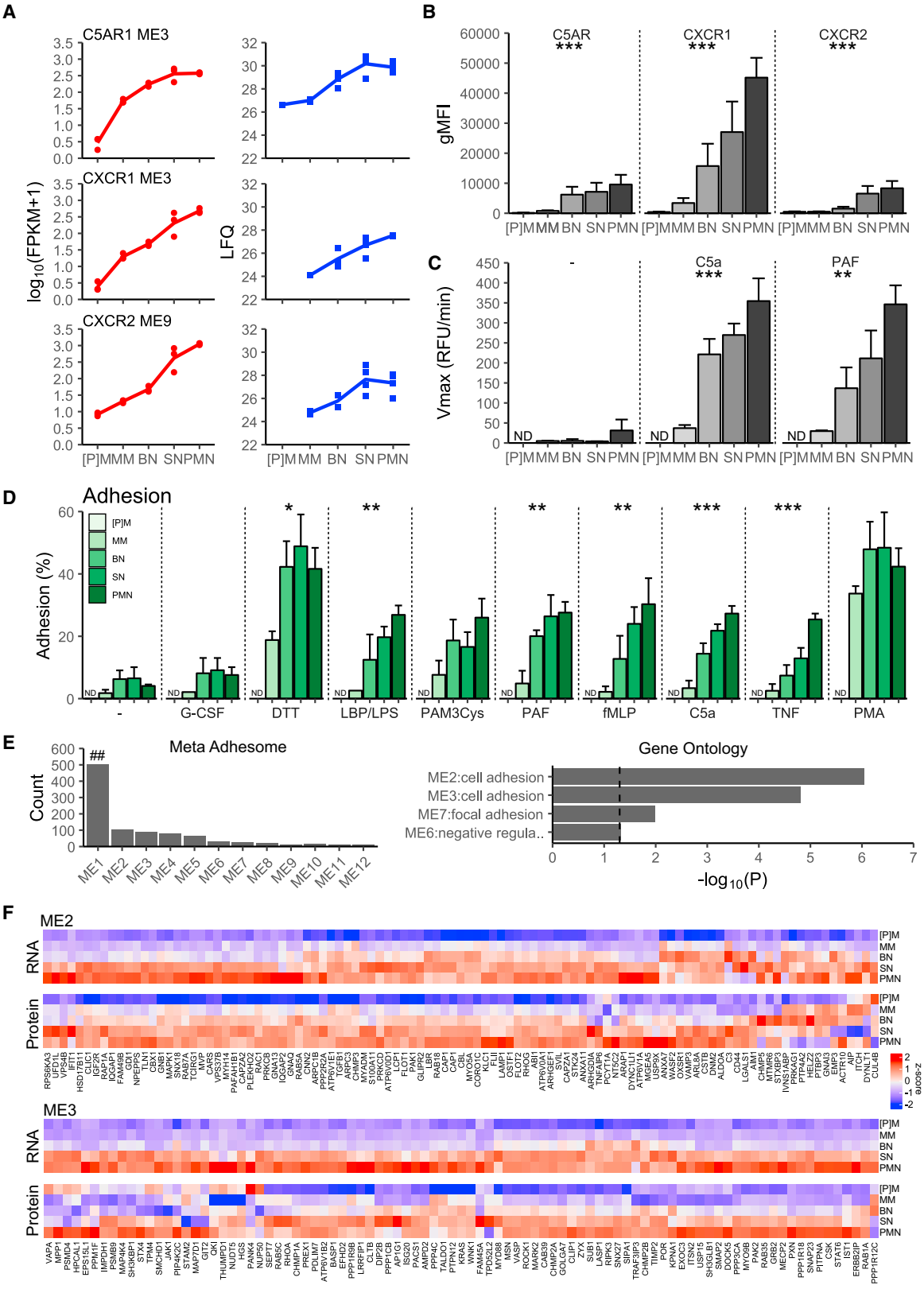

(legend on next page)

analysis confirmed that surface expression of the major chemotactic receptors, i.e., C5AR1, CXCR1, and CXCR2, increased from the BN stage to maximal expression in the bloodstream (all $p < 0.001$; Figures 5A and 5B). This corresponded with an increased cellular chemotactic response (Figure 5C). Surface expression of the chemokine receptor for neutrophil retention in the bone marrow, i.e., CXCR4 (Christopher and Link, 2007), remained low during all consecutive bone marrow stages of neutrophil development and could not be detected by proteomics, whereas transcriptome analysis suggested a modest if relevant increase (Grassi et al., 2018).

In agreement with the observed increase in chemotactic activity, adhesion increased during differentiation (Figure 5D). This corresponds with enrichment of the GO term adhesion in ME2, ME3, ME6, and ME7 (i.e., an increased phenotype) (Figure 5E), although the meta-adhesome database only enriched for ME1 (i.e., a decreased phenotype). ME2 and ME3 displayed the highest enrichment, and meta-adhesome-annotated proteins within these modules are plotted as heatmaps (Figure 5F). Notable members in these modules include CD44 and cytoskeletal elements of the Arp2/3 complex (ARPC1B and ARPC2) (Figure 5F). The role of ARPC1B expression in human neutrophil motility and lamellipodia formation (Kuijpers et al., 2017) and its profile upon differentiation are in agreement with our observation of chemotaxis and adhesion.

Thus, even in the general decrease in transcription and translation, the expression of essential components of the GPCRs, signaling, and cytoskeletal components required for directed motility seemed to be actively preserved from declining, if not selectively induced.

Production of Cytotoxic Proteins and Their Storage in Intracellular Vesicles

A hallmark of neutrophils is the ability to release an assortment of pre-stored antimicrobial proteins from various storage granules, including azurophilic granules (AGs), specific granules (SGs), gelatinase granules/ficolin-1-rich granules (GGs/FGs), and secretory vesicles (SVs). Granule proteins are used as markers for early neutrophil activation (e.g., MME [CD10]) or azurophilic granule release (CD63) (Kuijpers et al., 1991). The content of neutrophil granules has been shown to be controlled by a "targeting by timing" principle (Rørvig et al., 2013), in which the developmental stage at which a granule is formed determines its constituents. Previously, Rørvig et al. (2013) applied subcellular fractionation to annotate proteins to five granule subsets. In our dataset, 715 granule-annotated transcript-protein pairs showed changed expression profiles during differentiation (Table S1).

In agreement with protein storage, AG, SG, GG, and FG protein profiles showed either increasing abundance or consistently high protein levels, whereas RNA expression patterns were more variable (ranging from decreased, transiently increased, and sustained increased) (Figure S5). From these data, it appeared that the AG was synthesized before the [P]M stage and that protein levels of canonical azurophilic granule proteins (e.g., MPO and ELANE) remained stable during differentiation. In agreement with the concept of targeting by timing, the different granule subsets enriched in different transcriptome-proteome modules (Figure 6A), and key components of AGs, SGs, GGs/FGs, and SVs demonstrated distinct patterns of RNA and protein expression profiles (Figure S5). ME6 specifically enriched for SG-annotated proteins (Figure 6B); these granules develop after the azurophilic granules and display maximal RNA levels at the metamyelocyte stage (Figure 6C). Of the 121 transcript-protein pairs within ME6, 76 annotated as granule proteins, 22 were annotated with other functions (Table S1), and 23 were not annotated with the databases used in this study (Figure 6D). Therefore, the latter two groups contain potential novel SG proteins and are listed in Figure 6E.

These results are in line with our previous experiments, in which we measured the azurophil granule release reaction by the probe DQ-BSA, which becomes fluorescent upon cleavage by ELANE and/or cathepsin G (CTSG), two of the four major serine proteases from the AG. In further agreement with our mass spectrometry data, Triton TX-100 control values indicated that AGs are present from the [P]M stage onward (Grassi et al., 2018). However, degranulation upon activation by fMLP was only observed from the band stage onward. This coincides with initiation of FPR1 expression (Grassi et al., 2018) and indicates that the fMLP signaling cascade operates only at the final stages of differentiation.

ROS Formation: Final Accomplishment

In contrast to granule formation dynamics (Figure 6), the NADPH oxidase components for the generation of reactive oxygen species (ROS) behaved differently during neutrophil development. In addition to the membrane-associated heterodimer cytochrome b558, consisting of CYBA (p22phox) and CYBB (gp91phox),

Figure 5. Development of Chemotaxis and Adhesion Properties

(A) Line and dot plots of $\log_{10}$(FPKM+1) RNA expression and $\log_2$(LFQ) protein levels of C5AR1, CXCR1, and CXCR2 GPCRs.

(B) Flow cytometry analysis of CXCR1, CXCR2, and C5aR in bone marrow neutrophil progenitor fractions, showing gMFIs normalized to isotope control (n = 6 biological replicates measured in duplicate).

(C) Chemotaxis over 3 μm pore-size filters after C5a or PAF stimulation (n = 3 biological replicates measured in duplicate).

(D) Percentage of adhesion of calcein-labeled neutrophil progenitor cells, stimulated with 20 ng/mL of granulocyte-colony stimulating factor (G-CSF), 10 mmol/L of DTT, 20 μg/mL of Pam3Cys, 20 ng/mL of LPS in the presence of 50 ng/mL of LPS binding protein, 1 μmol/L of PAF, 10 nmol/L of C5a, 1 μmol/L of fMLP, 10 ng/mL of tumor necrosis factor alpha (TNF-α), or 100 ng/mL of PMA, to an uncoated 96-well maxisorp plate, determined as percentage of total input of calcein-labeled cells (n = 3 biological replicates measured in duplicate).

(E) Module membership distribution enrichment of adhesome-annotated proteins and highest enriched Gene Ontology terms containing "adhesion" in the description. Dashed line indicates the statistical significance threshold.

(F) Heatmap of meta-adhesome-annotated transcript-protein pairs in modules 2 and 3.

$^{*}p < 0.05$, $^{**}p < 0.01$, $^{***}p < 0.001$ as determined by ANOVA. $^{\#\#}p < 0.01$ as assessed with Fisher's exact tests. RFU, relative fluorescence unit. Summarizing data are depicted as mean + SD.

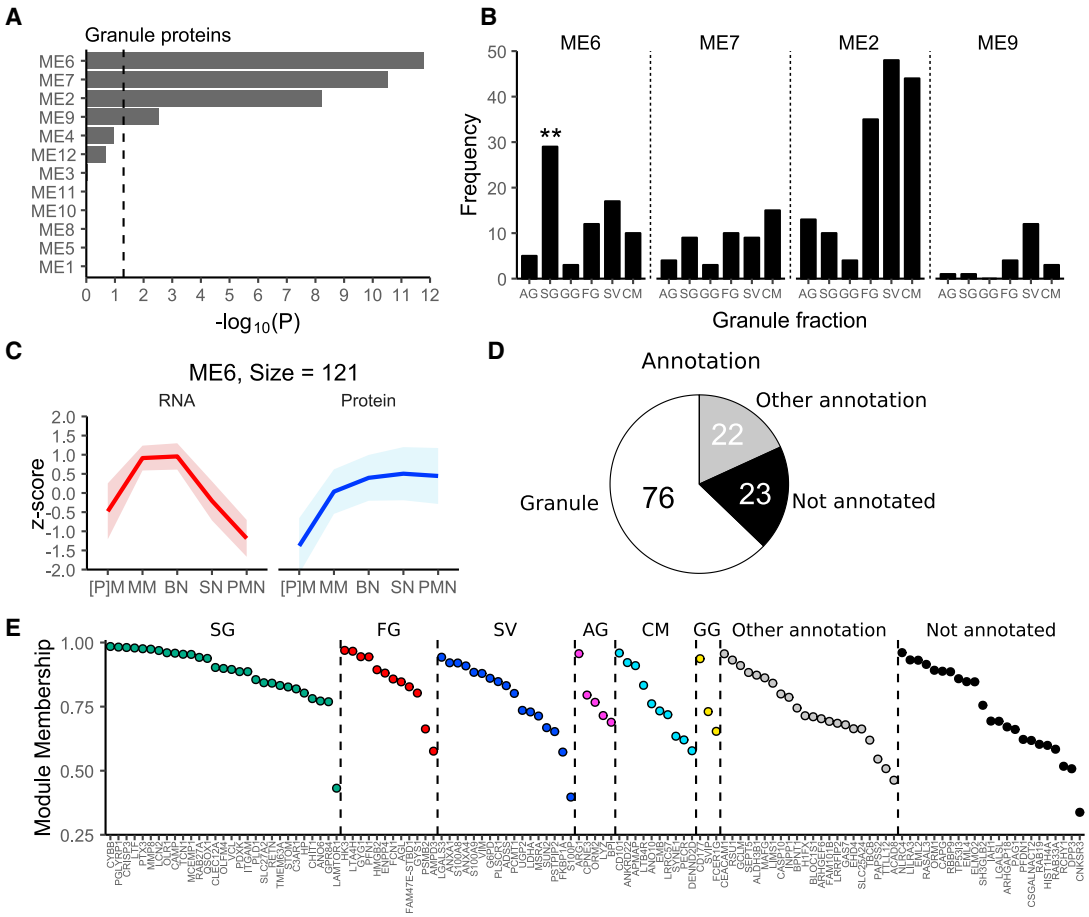

Figure 6. Granules

(A) Bar graph representing enrichment of transcript-protein pairs with granule annotation based on Rørvig et al. (2013). Dashed line depicts the statistical significance threshold.

(B) Distribution and enrichment of granule type annotations of functional modules enriched for granule proteins.

(C) Dynamics of transcripts and proteins in module 6.

(D) Pie graph showing amount of proteins within module 6 annotated as granule protein, annotated as having another function, or not annotated based on the databases used in this study.

(E) Transcript-protein pairs within module 6 are shown as a dot plot of decreasing rank of module membership, with groups per annotation sorted on median module membership. Colors represent annotation status.

**$p < 0.01$ as determined with Fisher's exact tests. Lines represent means; ribbons represent SDs. AG, azurophilic granule; SG, specific granule; GG, gelatinase granule; FG, ficolin-1-rich granule; SV, secretory vesicle; CM, cellular membrane. See also Figure S5 and Table S1.

the cytosolic proteins NCF1 (p47phox), NCF2 (p67phox), and NCF4 (p40phox) are involved in this process. Whereas protein levels of RAC1 and RAP1A did not change during differentiation, the presence of the most relevant small guanosine triphosphatase (GTPase) RAC2 involved in ROS formation in neutrophils (Ambruso et al., 2000) could not be detected by mass spectrometry, because we were unable to detect more than one peptide for RAC1-RAC2 differentiation needed for stringent protein quantification. CYBA (p22phox) and CYBB (gp91phox) were upregulated mainly during the transition from (pro)myelocyte to metamyelocyte. Although RNA levels for CYBA (p22phox) were stable, protein levels increased only after CYBB (gp91phox) protein was present, confirming complex assembly with the latter stabilizing CYBA (p22phox) (Roos et al., 1996) (Figure S6). The abundance of NCF1 (p47phox), NCF2 (p67phox), and NCF4 (p40phox) did increase more linearly (Figure S6).

Congenital Neutropenia and Neutrophil Disorders

Our data also allow examination of the dynamics in transcript-protein pairs regarding genes associated with congenital neutropenia and neutrophil disorders (Bousfiha et al., 2015; Picard et al., 2015). We observed 88 altered transcript-protein pairs related to primary immunodeficiency (PID)-annotated genes (Figure S7A). Of the obtained co-expression functional modules, ME2 enriched significantly for PID gene annotations (Figure S7B). Interestingly, absence of PID genes associated with congenital neutropenia in this analysis suggests that proteins that are essential for neutrophil development are expressed before the

promyelocyte stage, including ELANE, which accounts for up to 60% of cases of severe congenital neutropenia. Expression of PID genes that are associated with neutrophil dysfunction seems to be coordinated after the (pro)myelocyte stage during development. These include proteins associated with NADPH oxidase (p22phox/gp91phox protein [ME6 and ME7] and p47phox/p67phox/p40phox proteins [ME2]), signal transduction (PRKCD and STK4), adhesion and chemotaxis (ITGB2 and ME7), and granule release (STX11/STXBP2/MYO5A [ME2] and RAB27A [ME6]). In accordance, the corresponding genes were found to be regulated via transcriptional enhancer commitment at the final stages of neutrophil development (Grassi et al., 2018).

DISCUSSION

Granulopoiesis faces the challenge to daily produce a large number of cells that contain great amounts of cytotoxic proteins. Once released into the circulation, these cells migrate toward their targets to fulfill their deadly or damaging potential, being attracted by infectious agents or inflammatory triggers from activated tissues, including certain tumors. However, the dynamic changes that accompany the metamorphosis from a dividing myeloid progenitor cell in the bone marrow into a mature nondividing polymorphonuclear blood cell have remained poorly defined.

In this study, we reveal critical aspects of the rapid transformation from a dividing myeloid progenitor cell into an end-stage toxic effector neutrophil. Neutrophils express a limited number of highly abundant proteins that make up most of their total protein copy numbers, which is in agreement with the recent report of Rieckmann et al. (2017) on blood neutrophils. Our study extends and complements these data with a proteomic analysis of a unique set of five primary stages in human neutrophil development and by integrating these with deep sequencing data of these same subsets that were generated in parallel under identical circumstances (Grassi et al., 2018).

Most other studies on neutrophil differentiation have focused on transcriptomic signatures. It has been suggested that transcript expression in a gene-specific manner may be used as a proxy for protein levels (Edfors et al., 2016; Wilhelm et al., 2014). However, there are also reports of pervasive discordance of mRNA and protein levels during differentiation (Liu et al., 2016). By applying co-expression analysis on RNA and protein data simultaneously, we show the occurrence of both classical patterns of post-transcriptional regulation, in which an increase or a decrease in RNA expression preceded or coincided with a respective increase or decrease in protein abundance, as well as kinetic patterns that were highly variable between different genes and proteins.

The [P]M phase is the final stage in neutrophil development at which cell division occurs, and the subsequent loss of proliferative capacity constitutes a key step in the commitment to the myeloid lineage (Grassi et al., 2018). We show that this transition to mature neutrophils is accompanied by a strong decrease the abundance of proteins (in addition to transcripts) related to general cellular processes, such as DNA replication and repair, RNA transcription and processing, protein translation, and mitochondrial energy metabolism. These observations correspond to the well-described features of the end-stage bloodstream neutrophil. For instance, the decrease ribosomal proteins levels are in line with the low overall translational capacity of mature neutrophils. Moreover, our observation of diminished mitochondrial proteins levels corresponds with the described overall decreased mitochondrial mass in neutrophils (Maianski et al., 2004). Mature neutrophil mitochondrial remnants are morphologically distinct from classic mitochondria, and instead of mainly providing energy, these mitochondria fulfill an essential role in the characteristic spontaneous cell death of mature neutrophils once released from the bone marrow (Maianski et al., 2002; Murphy et al., 2003; van Raam et al., 2008). In agreement with our developmental stages in neutrophil development, it has previously been shown that during *in vitro* differentiation of the myeloid HL-60 cell line into mature neutrophil-like cells, the mitochondrial supercomplex organization is lost while aerobic glycolysis is increased (van Raam et al., 2008). Furthermore, an *in vivo* transcriptome and CyTOF study on murine granulopoiesis (Evrard et al., 2018) also indicated general DNA replication, RNA expression, and protein translation block in early neutrophil differentiation. Nonsense-mediated RNA decay was shown to play a role in granulocyte gene regulation (Wong et al., 2013). In this study, intron retention was found to be a mechanism to downregulate protein expression. When overlaying the transcripts identified to exhibit intron retention in neutrophils to our data, these also enriched in MEs that describe increased RNA and protein abundances (e.g., ME2; data not shown). Therefore, we cannot with certainty indicate whether this process also regulates downregulation or proteins in our study. Finally, our observation of reduced ribosomal protein abundance reflects previous electron microscopy (EM) observations that indicated a loss of endoplasmic reticulum (Bainton et al., 1971). Altogether, during neutrophil development there is a collapse of cell-cycle, transcriptional, mitochondrial, and metabolic activity.

Paradoxically, despite this strong decrease in biosynthesis potential, both the present study and the previously discussed murine study (Evrard et al., 2018) demonstrate that a specific subset of proteins is being produced, with peak abundancies at the final neutrophil developmental stages. These proteins are required for the typical activities associated with end-stage neutrophil effector function. An example of this is the NADPH oxidase enzyme complex. This machinery is needed to generate large amounts of ROS for neutrophil-mediated killing of pathogens, and it is only induced at the last stages of differentiation (Grassi et al., 2018). The myeloid capacity of toxic ROS induction seems programmed such that apart from the components of the enzyme complex, the receptors and signaling machinery to activate ROS production are expressed only late during development. Although it is tempting to speculate that these measures protect the bone marrow niche from inadvertently strong neutrophil activation within the local niche during infection of tissue damage elsewhere in the body, it was recently described that ROS production is required for reactive granulopoiesis in inflammatory conditions (Zhu et al., 2017).

In extreme circumstances, e.g., sepsis, apart from mature neutrophils, large amounts of immature neutrophils with a band-formed nucleus are present in the circulation (Mare et al., 2015). One could speculate that these immature cells may hold

merit in their higher metabolism and synthesis capacity. However, while they may lack a large capability to produce proteins, including antimicrobials, mature neutrophils are loaded with toxic payloads, forgoing the need for *de novo* translation. Moreover, from our chemotaxis analysis, mature neutrophils by far exceed immature cells in their capacity to show chemotaxis and a respiratory burst (Grassi et al., 2018). Therefore, the presence of immature neutrophils with a band-formed nucleus in the circulation in critical illness most likely represents the attempt to combat invading pathogens by a swift increase in cell numbers, rather than a well-regulated host response to return to homeostasis. The discrepancy between a general decline in RNA transcription and protein translation machinery, on the one hand, and increased levels of a subset of proteins, on the other hand, could be explained either by modulation of mRNA stability or by enhanced translation for only this select set of proteins. Regulation through translational control can be exerted by two mechanisms. First, altering the activity of the core translation machinery (i.e., ribosomal proteins) would influence the translational efficiency of most transcripts in the cell. Second, changing the activity of a subset of ribosomal proteins and/or RNA binding proteins that bind to regulatory sites in the 5′ or 3′ UTRs of specific mRNA molecules could selectively alter the translation of a only subset of genes. The first scenario seems unlikely to be relevant in maturating neutrophils, because the ribosomal protein machinery is subject to a rapid decline in levels of ribosomal proteins. This argues for the second scenario of unique regulation of a subset of proteins during end-stage neutrophil differentiation and prompts further experimental study.

In addition to highly correlating RNA/protein patterns, we observed more complex RNA versus protein expression profiles that infer the existence of as-yet-unidentified feedback mechanisms. More specifically, for a subset of genes, we observed increased mRNA expression levels during later stages of differentiation that were not accompanied by an increase in protein abundance. This suggests that mRNA may be pre-synthesized for rapid protein expression upon neutrophil activation or extravasation.

The converse kinetics were also observed, in which protein levels remained stable after RNA levels subsided. This could be indicative of protein stabilization by complex protein assembly as a mechanism to stabilize protein levels by protection from degradation. However, for a selection of several of these proteins, the large discrepancy between mRNA and protein expression could be explained by intracellular storage in granular structures, hence explaining their morphology and name as granulocytes.

The distinct dynamics of discordance between RNA and protein levels not only can be used to deduce function but also—to a certain extent—provides information on protein localization. Illustrative of this is the shape of functional module 6. This module enriched highly for granule protein annotations and in particular for SG proteins. Careful assessment of the members of this module revealed some bona fide SG granule proteins that were not annotated as such in the study by Rørvig et al. (2013), including membrane-expressed CEACAM1 and soluble ORM1. Other transcript-protein pairs, without granule annotation, that followed these dynamics included, upon manual investigation, proteins associated with granule trafficking and GTPase/vesicle transport. Therefore, the transcript-protein dynamics described in module 6 groups not only granule constituents but also proteins with a functional link with granule function or formation.

Our study has limitations. Enrichment on Gene Ontology and published databases were applied in our data analyses. However, these databases are often non-comprehensive and may not be directly in agreement with one another. An example of this is in the meta-adhesome database, which is based on human malignant melanoma (A375), human foreskin fibroblast (HFF), human chronic myelogenous leukemia (K562), mouse kidney fibroblast (MKF) cells, and mouse embryonic fibroblast (MEF) cells. Therefore, this database does not included important neutrophil proteins, e.g., integrins ITGAM and ITGB2. In contrast, these proteins were enriched in adhesion associated GO terms. Although samples for RNA-seq and proteomics analyses were from the same subsets, these were not obtained from the same sample; therefore, donor to donor differences may have an effect on our dataset. In addition, although for proteomics experiments each group consists of 4 samples, there is inconsistency between biological and technical replicates because of the difficulty of obtaining sufficiently large primary human bone marrow samples for sorting into the progenitor cell fractions for proteomics analysis. [P]Ms were obtained from 2 individuals, the MM subset was obtained from 3 individuals, BNs were obtained from 3 individuals, SNs were obtained from 2 individuals, and PMNs were obtained from 4 individuals. This limited biological diversity may influence the robustness of our analysis and would likely benefit from independent validation in separately obtained samples. Another limitation is that while ANOVA enables testing for changes in the continuous differentiation of our samples, it does not directly enable to pinpoint at which stage this effect was present.

Overall, our findings reinforce the notion that temporal analysis of mRNA and protein profiles is more informative than steady-state profiling and that systems biology approaches are a powerful supplement to "one gene, one protein" studies. Our integrated transcript-protein analysis describes the flow from RNA to protein for a large portion of genes and proteins during neutrophil differentiation, underpinning neutrophil biology as it is known to date. Therefore, we here provided a resource to generate and test new biological hypotheses and demonstrated a highly heterogeneous and flexible system of cell differentiation, changing from dividing, non-toxic precursor cells to mobile, toxic effector cells.

STAR★METHODS

Detailed methods are provided in the online version of this paper and include the following:

- KEY RESOURCES TABLE
- LEAD CONTACT AND MATERIALS AVAILABILITY
- EXPERIMENTAL MODEL AND SUBJECT DETAILS
- METHOD DETAILS
  - Sample preparation for mass spectrometry analysis
  - Mass spectrometry data acquisition
  - Flow cytometry
  - Functional assays

SUPPLEMENTAL INFORMATION

Supplemental Information can be found online at https://doi.org/10.1016/j.celrep.2019.10.082.

ACKNOWLEDGMENTS

The work presented here was supported by the Landsteiner Foundation for Blood Transfusion Research (LSBR-1517 and LSBR-1121 to M.v.d.B. and F.P., respectively) and by the Sanquin Blood Supply Product and Process Development Cellular Poducts Fund (PPOC-2089 and PPOC-1873 to C.E.M.A. and I.H.H., respectively). M.F. is supported by the British Heart Foundation (FS/18/53/33863). We thank Dr. Dirk Roos and Dr. Marieke von Lindern for critical reading of the manuscript.

AUTHOR CONTRIBUTIONS

A.J.H., M.v.d.B., and T.W.K. designed the study, performed experiments, supervised research, analyzed data, and wrote the manuscript. F.P. designed the study, performed experiments, and analyzed data. L.G. analyzed data. C.E.M.A., A.T.J.T., and I.H.H. performed experiments and analyzed data. M.F. supervised research and wrote the manuscript. A.B.M. supervised research. All authors read and approved the final version of the manuscript.

DECLARATION OF INTERESTS

The authors declare no competing interests.

Received: May 13, 2019
Revised: July 10, 2019
Accepted: October 21, 2019
Published: November 26, 2019

REFERENCES

Ambruso, D.R., Knall, C., Abell, A.N., Panepinto, J., Kurkchubasche, A., Thurman, G., Gonzalez-Aller, C., Hiester, A., deBoer, M., Harbeck, R.J., et al. (2000). Human neutrophil immunodeficiency syndrome is associated with an inhibitory Rac2 mutation. Proc. Natl. Acad. Sci. USA *97*, 4654–4659.

Bainton, D.F., Ullyot, J.L., and Farquhar, M.G. (1971). The development of neutrophilic polymorphonuclear leukocytes in human bone marrow. J. Exp. Med. *134*, 907–934.

Borregaard, N. (2010). Neutrophils, from marrow to microbes. Immunity *33*, 657–670.

Bousfiha, A., Jeddane, L., Al-Herz, W., Ailal, F., Casanova, J.L., Chatila, T., Conley, M.E., Cunningham-Rundles, C., Etzioni, A., Franco, J.L., et al. (2015). The 2015 IUIS Phenotypic Classification for Primary Immunodeficiencies. J. Clin. Immunol. *35*, 727–738.

Calvo, S.E., Clauser, K.R., and Mootha, V.K. (2016). MitoCarta2.0: an updated inventory of mammalian mitochondrial proteins. Nucleic Acids Res. *44* (*D1*), D1251–D1257.

Christopher, M.J., and Link, D.C. (2007). Regulation of neutrophil homeostasis. Curr. Opin. Hematol. *14*, 3–8.

Cox, J., and Mann, M. (2008). MaxQuant enables high peptide identification rates, individualized p.p.b.-range mass accuracies and proteome-wide protein quantification. Nat. Biotechnol. *26*, 1367–1372.

Damiano, V.V., Kucich, U., Murer, E., Laudenslager, N., and Weinbaum, G. (1988). Ultrastructural quantitation of peroxidase- and elastase-containing granules in human neutrophils. Am. J. Pathol. *131*, 235–245.

Dancey, J.T., Deubelbeiss, K.A., Harker, L.A., and Finch, C.A. (1976). Neutrophil kinetics in man. J. Clin. Invest. *58*, 705–715.

Duarte, N.C., Becker, S.A., Jamshidi, N., Thiele, I., Mo, M.L., Vo, T.D., Srivas, R., and Palsson, B.O. (2007). Global reconstruction of the human metabolic network based on genomic and bibliomic data. Proc. Natl. Acad. Sci. USA *104*, 1777–1782.

Edfors, F., Danielsson, F., Hallström, B.M., Käll, L., Lundberg, E., Pontén, F., Forsström, B., and Uhlén, M. (2016). Gene-specific correlation of RNA and protein levels in human cells and tissues. Mol. Syst. Biol. *12*, 883.

Evrard, M., Kwok, I.W.H., Chong, S.Z., Teng, K.W.W., Becht, E., Chen, J., Sieow, J.L., Penny, H.L., Ching, G.C., Devi, S., et al. (2018). Developmental Analysis of Bone Marrow Neutrophils Reveals Populations Specialized in Expansion, Trafficking, and Effector Functions. Immunity *48*, 364–379.

Gerstberger, S., Hafner, M., and Tuschl, T. (2014). A census of human RNA-binding proteins. Nat. Rev. Genet. *15*, 829–845.

Grassi, L., Pourfarzad, F., Ullrich, S., Merkel, A., Were, F., Carrillo-de-Santa-Pau, E., Yi, G., Hiemstra, I.H., Tool, A.T.J., Mul, E., et al. (2018). Dynamics of Transcription Regulation in Human Bone Marrow Myeloid Differentiation to Mature Blood Neutrophils. Cell Rep. *24*, 2784–2794.

Häger, M., Cowland, J.B., and Borregaard, N. (2010). Neutrophil granules in health and disease. J. Intern. Med. *268*, 25–34.

Heifets, L. (1982). Centennial of Metchnikoff's discovery. J. Reticuloendothel. Soc. *31*, 381–391.

Hentze, M.W., Castello, A., Schwarzl, T., and Preiss, T. (2018). A brave new world of RNA-binding proteins. Nat. Rev. Mol. Cell Biol. *19*, 327–341.

Horton, E.R., Byron, A., Askari, J.A., Ng, D.H.J., Millon-Frémillon, A., Robertson, J., Koper, E.J., Paul, N.R., Warwood, S., Knight, D., et al. (2015). Definition of a consensus integrin adhesome and its dynamics during adhesion complex assembly and disassembly. Nat. Cell Biol. *17*, 1577–1587.

Huber, W., Carey, V.J., Gentleman, R., Anders, S., Carlson, M., Carvalho, B.S., Bravo, H.C., Davis, S., Gatto, L., Girke, T., et al. (2015). Orchestrating high-throughput genomic analysis with Bioconductor. Nat. Methods *12*, 115–121.

Kolaczkowska, E., and Kubes, P. (2013). Neutrophil recruitment and function in health and inflammation. Nat. Rev. Immunol. *13*, 159–175.

Kuijpers, T.W., Tool, A.T., van der Schoot, C.E., Ginsel, L.A., Onderwater, J.J., Roos, D., and Verhoeven, A.J. (1991). Membrane surface antigen expression on neutrophils: a reappraisal of the use of surface markers for neutrophil activation. Blood *78*, 1105–1111.

Kuijpers, T.W., Tool, A.T.J., van der Bijl, I., de Boer, M., van Houdt, M., de Cuyper, I.M., Roos, D., van Alphen, F., van Leeuwen, K., Cambridge, E.L., et al. (2017). Combined immunodeficiency with severe inflammation and allergy caused by ARPC1B deficiency. J. Allergy Clin. Immunol. *140*, 273–277.e10.

Lahoz-Beneytez, J., Elemans, M., Zhang, Y., Ahmed, R., Salam, A., Block, M., Niederalt, C., Asquith, B., and Macallan, D. (2016). Human neutrophil kinetics: modeling of stable isotope labeling data supports short blood neutrophil half-lives. Blood *127*, 3431–3438.

Langfelder, P., and Horvath, S. (2008). WGCNA: an R package for weighted correlation network analysis. BMC Bioinformatics *9*, 559.

Lindeboom, R.G., van Voorthuijsen, L., Oost, K.C., Rodríguez-Colman, M.J., Luna-Velez, M.V., Furlan, C., Baraille, F., Jansen, P.W., Ribeiro, A., Burgering, B.M., et al. (2018). Integrative multi-omics analysis of intestinal organoid differentiation. Mol. Syst. Biol. *14*, e8227.

Liu, Y., Beyer, A., and Aebersold, R. (2016). On the Dependency of Cellular Protein Levels on mRNA Abundance. Cell *165*, 535–550.

Maianski, N.A., Mul, F.P., van Buul, J.D., Roos, D., and Kuijpers, T.W. (2002). Granulocyte colony-stimulating factor inhibits the mitochondria-dependent activation of caspase-3 in neutrophils. Blood *99*, 672–679.

Maianski, N.A., Geissler, J., Srinivasula, S.M., Alnemri, E.S., Roos, D., and Kuijpers, T.W. (2004). Functional characterization of mitochondria in neutrophils: a role restricted to apoptosis. Cell Death Differ. *11*, 143–153.

Mare, T.A., Treacher, D.F., Shankar-Hari, M., Beale, R., Lewis, S.M., Chambers, D.J., and Brown, K.A. (2015). The diagnostic and prognostic significance of monitoring blood levels of immature neutrophils in patients with systemic inflammation. Crit. Care *19*, 57.

Moulding, D.A., Quayle, J.A., Hart, C.A., and Edwards, S.W. (1998). Mcl-1 expression in human neutrophils: regulation by cytokines and correlation with cell survival. Blood *92*, 2495–2502.

Murphy, B.M., O'Neill, A.J., Adrain, C., Watson, R.W., and Martin, S.J. (2003). The apoptosome pathway to caspase activation in primary human neutrophils exhibits dramatically reduced requirements for cytochrome C. J. Exp. Med. *197*, 625–632.

Murthy, A.R., Lehrer, R.I., Harwig, S.S., and Miyasaki, K.T. (1993). *In vitro* candidastatic properties of the human neutrophil calprotectin complex. J. Immunol. *151*, 6291–6301.

Papayannopoulos, V., and Zychlinsky, A. (2009). NETs: a new strategy for using old weapons. Trends Immunol. *30*, 513–521.

Picard, C., Al-Herz, W., Bousfiha, A., Casanova, J.L., Chatila, T., Conley, M.E., Cunningham-Rundles, C., Etzioni, A., Holland, S.M., Klein, C., et al. (2015). Primary Immunodeficiency Diseases: an Update on the Classification from the International Union of Immunological Societies Expert Committee for Primary Immunodeficiency 2015. J. Clin. Immunol. *35*, 696–726.

Pillay, J., den Braber, I., Vrisekoop, N., Kwast, L.M., de Boer, R.J., Borghans, J.A., Tesselaar, K., and Koenderman, L. (2010). *In vivo* labeling with 2H2O reveals a human neutrophil lifespan of 5.4 days. Blood *116*, 625–627.

Rappsilber, J., Ishihama, Y., and Mann, M. (2003). Stop and go extraction tips for matrix-assisted laser desorption/ionization, nanoelectrospray, and LC/MS sample pretreatment in proteomics. Anal. Chem. *75*, 663–670.

Rieckmann, J.C., Geiger, R., Hornburg, D., Wolf, T., Kveler, K., Jarrossay, D., Sallusto, F., Shen-Orr, S.S., Lanzavecchia, A., Mann, M., and Meissner, F. (2017). Social network architecture of human immune cells unveiled by quantitative proteomics. Nat. Immunol. *18*, 583–593.

Roos, D., de Boer, M., Kuribayashi, F., Meischl, C., Weening, R.S., Segal, A.W., Ahlin, A., Nemet, K., Hossle, J.P., Bernatowska-Matuszkiewicz, E., and Middleton-Price, H. (1996). Mutations in the X-linked and autosomal recessive forms of chronic granulomatous disease. Blood *87*, 1663–1681.

Rørvig, S., Østergaard, O., Heegaard, N.H., and Borregaard, N. (2013). Proteome profiling of human neutrophil granule subsets, secretory vesicles, and cell membrane: correlation with transcriptome profiling of neutrophil precursors. J. Leukoc. Biol. *94*, 711–721.

Slenter, D.N., Kutmon, M., Hanspers, K., Riutta, A., Windsor, J., Nunes, N., Mélius, J., Cirillo, E., Coort, S.L., Digles, D., et al. (2018). WikiPathways: a multifaceted pathway database bridging metabolomics to other omics research. Nucleic Acids Res. *46* (*D1*), D661–D667.

Szatmary, A.C., Nossal, R., Parent, C.A., and Majumdar, R. (2017). Modeling neutrophil migration in dynamic chemoattractant gradients: assessing the role of exosomes during signal relay. Mol. Biol. Cell *28*, 3457–3470.

Thul, P.J., Åkesson, L., Wiking, M., Mahdessian, D., Geladaki, A., Ait Blal, H., Alm, T., Asplund, A., Björk, L., Breckels, L.M., et al. (2017). A subcellular map of the human proteome. Science *356*, eaal3321.

Tibshirani, R., Walther, G., and Hastie, T. (2001). Estimating the number of clusters in a data set via the gap statistic. J. R. Stat. Soc. Series B Stat. Methodol. *63*, 411–423.

Tyanova, S., Temu, T., Sinitcyn, P., Carlson, A., Hein, M.Y., Geiger, T., Mann, M., and Cox, J. (2016). The Perseus computational platform for comprehensive analysis of (prote)omics data. Nat. Methods *13*, 731–740.

van Raam, B.J., Verhoeven, A.J., and Kuijpers, T.W. (2006). Mitochondria in neutrophil apoptosis. Int. J. Hematol. *84*, 199–204.

van Raam, B.J., Sluiter, W., de Wit, E., Roos, D., Verhoeven, A.J., and Kuijpers, T.W. (2008). Mitochondrial membrane potential in human neutrophils is maintained by complex III activity in the absence of supercomplex organisation. PLoS ONE *3*, e2013.

Wilhelm, M., Schlegl, J., Hahne, H., Gholami, A.M., Lieberenz, M., Savitski, M.M., Ziegler, E., Butzmann, L., Gessulat, S., Marx, H., et al. (2014). Mass-spectrometry-based draft of the human proteome. Nature *509*, 582–587.

Wiśniewski, J.R., Zougman, A., Nagaraj, N., and Mann, M. (2009). Universal sample preparation method for proteome analysis. Nat. Methods *6*, 359–362.

Wiśniewski, J.R., Hein, M.Y., Cox, J., and Mann, M. (2014). A "proteomic ruler" for protein copy number and concentration estimation without spike-in standards. Mol. Cell. Proteomics *13*, 3497–3506.

Wong, J.J., Ritchie, W., Ebner, O.A., Selbach, M., Wong, J.W., Huang, Y., Gao, D., Pinello, N., Gonzalez, M., Baidya, K., et al. (2013). Orchestrated intron retention regulates normal granulocyte differentiation. Cell *154*, 583–595.

Yu, G., Wang, L.G., Han, Y., and He, Q.Y. (2012). clusterProfiler: an R package for comparing biological themes among gene clusters. OMICS *16*, 284–287.

Zhu, H., Kwak, H.J., Liu, P., Bajrami, B., Xu, Y., Park, S.Y., Nombela-Arrieta, C., Mondal, S., Kambara, H., Yu, H., et al. (2017). Reactive Oxygen Species-Producing Myeloid Cells Act as a Bone Marrow Niche for Sterile Inflammation-Induced Reactive Granulopoiesis. J. Immunol. *198*, 2854–2864.

STAR★METHODS

KEY RESOURCES TABLE

REAGENT or RESOURCE	SOURCE	IDENTIFIER
Antibodies		
human anti CD11b (clone ICRF44)	BD PharMingen	Cat#558123; RRID: AB_397043
Human anti CD16 (clone 3G8)	BD PharMingen	Cat# 557744; RRID: AB_396850
Human anti C5aR (clone 5/1)	Biolegend	Cat# 135805; RRID: AB_2067285
Human anti CXCR1 (clone 42705.111)	R and D Systems	Cat# MAB330; RRID: AB_2126479
Human anti CXCR2 (clone 48311.211)	R and D Systems	Cat#MAB331; RRID: AB_2296102
goat anti-mouse IgG	Life Technologies	CAT#A11001; RRID: AB_2534069
Biological Samples		
Bone marrow samples	Amsterdam UMC – location AMC – Patients undergoing surgery for unrelated, non-hematological procedures	N/A
Chemicals, Peptides, and Recombinant Proteins		
Mitotracker Green	Molecular Probes	Cat#M7514
Calcein-AM	Molecular Probes	Cat#C3100MP
G-CSF	Neupogen, clinical grade	N/A
LPS isolated from *E. coli* strain O55:B5	Sigma Aldrich	Cat#L2880
LBP	R&D Systems	Cat#870-LP-025
C5a	Sino Biological Inc	Cat#10604-HNAE
fMLP	Sigma Aldrich	Cat#F3506
TNFα	Peprotech	Cat#300-01A
PMA	Sigma	Cat#P8139
PAF	Sigma	Cat#P4904
Pam3Cys	EMC Microcollections	Cat#L2000
Critical Commercial Assays		
EasySep Human Neutrophil Enrichment Kit	STEMCELL Technologies	Cat#19257
Deposited Data		
Raw and analyzed MS data	This paper	PXD013785
Uniprot database (release 2015—02, 89796 entries)	The UniProt consortium	https://www.uniprot.org
Software and Algorithms		
Maxquant 1.5.2.8	Cox and Mann, 2008	https://maxquant.net/maxquant/
Perseus 1.5.1.6	Tyanova et al., 2016	https://maxquant.net/perseus/
R 3.5.2	R Core Team, R Foundation for Statistical Computing,Vienna, Austria	https://cran.r-project.org/
Bioconductor 3.6	Huber et al., 2015	https://www.bioconductor.org/
Rstudio 1.1.456	Rstudio Team, 2016	https://rstudio.com/
Xcalibur 4.1.31.9	Thermo Scientific	https://www.thermofisher.com/us/en/home.html
FlowJo 10	FlowJo LCC	https://www.flowjo.com/
Other		
Cluster of differentiation annotation database	Human protein atlas	https://www.proteinatlas.org/
GPCR annotation database	Human protein atlas	https://www.proteinatlas.org/
FDA approved targets annotations	Human protein atlas	https://www.proteinatlas.org/
Transcription factor annotations	Human protein atlas	https://www.proteinatlas.org/

(*Continued on next page*)

Continued

REAGENT or RESOURCE	SOURCE	IDENTIFIER
Ribosomal proteins annotations	Human protein atlas	https://www.proteinatlas.org/
Granule protein annotations	Rørvig et al., 2013	http://doi.wiley.com/10.1189/jlb.1212619
Meta Adhesome annotations	Horton et al., 2015	http://www.nature.com/articles/ncb3257
Primary immunodeficiency genes annotations	Picard et al., 2015	http://link.springer.com/10.1007/s10875-015-0201-1
RNA binding protein annotations	Gerstberger et al., 2014	http://www.nature.com/articles/nrg3813
RECON1 database	Duarte et al., 2007	http://www.pnas.org/cgi/doi/10.1073/pnas.0610772104
MitoCarta 2.0 database	Calvo et al., 2016	https://academic.oup.com/nar/article-lookup/doi/10.1093/nar/gkv1003

LEAD CONTACT AND MATERIALS AVAILABILITY

Further information and requests for resources and reagents should be directed to and will be fulfilled by the Lead Contact, T.W. Kuijpers (t.w.kuijpers@amsterdamumc.nl). This study did not generate new unique reagents.

EXPERIMENTAL MODEL AND SUBJECT DETAILS

The study was approved by the local ethical committee of Sanquin Blood Supply Organization, and the Academic Medical Center (AMC), Amsterdam, the Netherlands. Bone marrow samples were obtained from individuals considered to be healthy, undergoing surgery for unrelated, non-hematological procedures after obtaining written informed consent according to the Helsinki protocol. Mature neutrophils were collected from other different healthy donors. Samples were anonymized for research, sex/gender and age information was unavailable. Peripheral blood was diluted 1:1 with PBS/TSC (tri-sodium citrate) and separated by gradient centrifugation (Percoll 1.076 g/ml). Neutrophils were isolated from the pellet after red cell lysis in ice-cold erythrocyte lysis buffer (150 mM NH_4Cl/10 mM $KHCO_3$/0.1 mM EDTA) and purified by negative selection with EasySep Human Neutrophil Enrichment Kit. The cells were re-suspended in HEPES medium (132 mM NaCl, 20 mM HEPES, 6 mM KCl, 1 mM $MgSO_4$, 1.2 mM K_2HPO_4), supplemented with 1 mM $CaCl_2$, 1 mg/ml glucose and 0.5% (w/v) human serum albumin, pH 7.4. For neutrophil progenitor purification, the remaining cells were re-suspended in HEPES medium at 10^7 cells per ml and stained with CD11b-APC (Clone D12, BD) and CD16-PE (Clone 3G8, BD) for 30 min, followed by one PBS wash and re-suspension in HEPES medium at 10^7 cells per ml. Subsequently, the cells were sorted on a BD FACSAria III cell sorter. The granulocyte gate (FSC-high/SSC-high) was sorted in to 4 different populations: CD11b−/CD16−, CD11b+/CD16−, CD11b+/CD16dim and CD11b+/CD16+. After cell sorting, cells were washed twice with PBS, the cell pellet was frozen in liquid nitrogen and stored at −80°C. [P]M cells were obtained from 2 individuals, the MM subset from 3 individuals, BN from 3 individuals, SN from 2 individuals and PMNs from 4 individuals. For all subpopulations 4 samples were analyzed (P[M] 2 biological replicates with 3 technical replicates of one donor, MM 3 biological replicates with 2 technical replicates of one donors, BN 3 biological replicates with 2 technical replicates of one donor, SN 2 biological replicates with 2 technical replicates of two donors and PMN 4 biological replicates).

METHOD DETAILS

Sample preparation for mass spectrometry analysis

Cell pellets were lysed in 30 μL of 4% SDS, 100 mM DTT, 100 mM Tris-HCl pH 7.5 supplemented with HALT protease and phosphatase inhibitor cocktail (Thermo Scientific). Tryptic peptides were obtained by means of the Filter Aided Sample Preparation method (Wiśniewski et al., 2009): samples were transferred to 30Kda filters (Millipore) and centrifuged twice after addition of 200 μL 8 M urea in 0.1 M Tris/HCl pH 8.5 for 30 minutes at 14000 x g. Next, 100 μL 0.055 iodoacetamide / 8 M urea in 0.1 M Tris/HCl pH 8.5 was added and incubated for 20 minutes at room temperature in the dark, subsequently centrifuged at 14000 x g for 30 minutes and after adding 100 μL 8 M urea in 0.1 M Tris/HCl pH 8.5 centrifuged at 14000 x g for 30 minutes. 0.05M NH_4HCO_3 was added and filters were centrifuged at 14000 x g for 30 minutes. Next, proteins digested overnight with trypsin (ratio 1:100, Promega) in 0.05M NH_4HCO_3. Peptides were obtained by centrifuging the filter units at 2500 x g for 20 min. For desalting, samples were loaded on methanol activated Empore-C18 StageTips (Rappsilber et al., 2003), centrifuged at 200 x g for 7 minutes; washed twice with 0.5% acetic acid and eluted with 0.5% acetic acid/80% acetonitrile. Sample volume was reduced by SpeedVac and supplemented with 2% acetonitrile, 0.1% TFA to a final volume of 12 μl. For each sample, 3 technical replicates were analyzed by injecting 3 μL of the sample.

Mass spectrometry data acquisition

Tryptic peptides were separated by nanoscale C18 reverse chromatography coupled on line to an Orbitrap Fusion Tribrid mass spectrometer (Thermo Scientific) via a nanoelectrospray ion source (Nanospray Flex Ion Source, Thermo Scientific). Peptides were loaded on a 20 cm 75–360 μm inner-outer diameter fused silica emitter (New Objective) packed in-house with ReproSil-Pur C18-AQ, 1.9 μm resin (Dr Maisch GmbH). The column was installed on a Dionex Ultimate3000 RSLC nanoSystem (Thermo Scientific) by means of a MicroTee union formatted for 360 μm outer diameter columns (IDEX) and a liquid junction. The spray voltage was set to 2.15 kV. Buffer A was composed of 0.5% (v/v) acetic acid and buffer B of 0.5% (v/v) acetic acid, 80% (v/v) acetonitrile. Peptides were loaded for 17 min at 300 nl/min at 5% buffer B, equilibrated for 5 minutes at 5% buffer B (17-22 min) and eluted by increasing buffer B from 5%–15% (22-87 min) and 15%–38% (87-147 min), followed by a 10 minute wash to 90% and a 5 min regeneration to 5%. Survey scans of peptide precursors from 400 to 1500 m/z were performed at 120K resolution (at 200 m/z) with a 1.5×10^5 ion count target. Tandem mass spectrometry was performed by isolation with the quadrupole with isolation window 1.6, HCD fragmentation with normalized collision energy of 30, and rapid scan mass spectrometry analysis in the ion trap. The MS^2 ion count target was set to 10^4 and the max injection time was 35 ms. Only those precursors with charge state 2–7 were sampled for MS^2. The dynamic exclusion duration was set to 60 s with a 10 ppm tolerance around the selected precursor and its isotopes. Monoisotopic precursor selection was turned on. The instrument was run in top speed mode with 3 s cycles. All data were acquired with Xcalibur software.

Flow cytometry

Single-cell bone marrow suspensions were labeled with Pacific Blue-labeled anti-human CD11b (clone ICRF44, BD PharMingen) and PE-Cy7-labeled anti-human CD16 (clone 3G8, BD PharMingen) to discriminate the different neutrophil progenitor stages. In addition the cells were stained with PE-labeled anti-human C5aR (clone 5/1, Biolegend) and either anti-human CXCR1 (clone 42705.111, R&D) or anti-human CXCR2 (clone 48311.211, R&D) followed by 2^{nd} antibody staining of Alexa Fluor488 goat anti-mouse IgG (Life Technologies). Samples were measured on a Canto II cytometer (BD Biosciences) and analyzed with FlowJo software (Ashland, OR, USA).

Functional assays

Neutrophil adhesion and chemotaxis were analyzed as described (Kuijpers et al., 2017) and detailed here. To investigate neutrophil adhesion, neutrophil progenitor cells (5×10^6/mL) were incubated with calcein-AM (4 ug/ml final concentration; Molecular Probes) for 30 minutes at 37°C, washed twice, and resuspended in HEPES buffer at a concentration of 2×10^6/mL. Adhesion was determined in an uncoated 96-well MaxiSorp plate (Nunc, Wiesbaden, Germany). Calcein-labeled neutrophil progenitor cells (2×10^5/well, final volume 100 μL) were stimulated with one of the following: granulocyte-colony stimulating factor (G-CSF) (20 ng/mL), 10 mmol/L dithiothreitol ([DTT]; Sigma Aldrich, St Louis, Mo), 20 mg/mL Pam3Cys (EMC Microcollections, Tübingen, Germany), 20 ng/mL bacterial Toll-like receptor-4 ligand LPS (isolated from *E. coli* strain 055:B5; Sigma Aldrich) in the presence of 50 ng/mL LPS binding protein (R&D Systems, Minneapolis, Minn), 1 mmol/L PAF (Sigma Aldrich), 10 nmol/L C5a (Sigma Aldrich), 1 mmol/L fMLP, TNF-a (10 ng/mL), or 100 ng/mL PMA. Plates were incubated for 30 minutes at 37°C and washed 3 times with PBS. Adherent cells were lysed in 0.5% (wt/vol) Triton X-100 in H_2O for 5 minutes at room temperature. Fluorescence was measured with a Tecan Infinite F200-pro plate reader at an excitation wavelength of 485 nm and an emission wavelength of 535 nm. Adhesion was determined as percentage of total input of calcein-labeled cells. Neutrophil chemotaxis was measured with 3-μm pore-size Fluoroblock inserts (Corning Inc, Corning, NY), in a Falcon 24-well plate. Calcein-labeled PMNs (2×10^6/mL, 0.3 mL) were pipetted in the insert (upper compartment), and placed in the lower compartment containing 0.8 mL of C5a (10^{-8} mol/L) or PAF (10^{-7} mol/L). Fluorescence was measured underneath the filter every 2.5 minutes for 45 minutes with a Tecan Infinite F200-pro plate reader at an excitation wavelength of 485 nm and an emission wavelength of 535 nm. Mitochondria were stained using about 10^5 [P]Ms or PMNs, these were incubated in IMDM for 30 minutes in a 5% CO2 incubator at 37°C with 100 nmol/L MitoTracker Green. Next, cells were pelleted, resuspended in 30 μL stain-free medium and placed on microscope glass slides (Maianski et al., 2002).

QUANTIFICATION AND STATISTICAL ANALYSIS

Mass spectrometry data analysis

The RAW mass spectrometry files were processed with the MaxQuant computational platform, 1.5.2.8(Cox and Mann, 2008). Proteins and peptides were identified with the Andromeda search engine by querying the human Uniprot database (release 2015—02, 89796 entries). Standard settings with the additional options match between runs, Label Free Quantification (LFQ), and unique peptides for quantification were selected. The generated 'proteingroups.txt' table was filtered for potential contaminants, reverse hits and 'only identified by site' by Perseus 1.5.1.6 (Tyanova et al., 2016). The LFQ values were transformed in $\log_2$ scale, the three technical replicates per experimental condition grouped and averaged based on the median, and proteins were filtered for at least two valid values in one of the experimental groups. Missing values were imputed by normal distribution (width = 0.3, shift = 1.8), assuming these proteins were close to the detection limit. LFQ values were transformed to estimated absolute copy numbers by means of the proteomic ruler methodology (Wiśniewski et al., 2014). To identify the proteins with the most prominent differences expression profiles within the different neutrophil progenitor cell subsets, we used the built-in ANOVA function in PERSEUS using an FDR of 5% and S0 of 0.4. For all subpopulations 4 samples were analyzed (as described in detail in the *Experimental Model and Subject Details*). All

following analyses were performed in R/Bioconductor (versions 3.5.2/3.6). Clustering was performed with K-means with an optimal number of clusters (K) determined with gap statistics (Tibshirani et al., 2001).

Transcript-Protein co-expression network analysis

Overall changes in median FPKM of transcripts defined as protein coding, FPKM > 1, corresponding to identified and quantified proteins were determined by ANOVA with a Tukey post-test. Proportional comparison in were performed with Fisher exact tests. To assess transcriptome and proteome dynamics were evaluated by means of weighted gene co-expression network analysis (WGCNA)(Langfelder and Horvath, 2008; Rieckmann et al., 2017). Transcript-protein pairs for which either protein (ANOVA, FDR < 0.05, S0 = 0.4) or RNA (posterior probability > 0.5, absolute fold change > 2 and FPKM > 1) (Grassi et al., 2018)) was significantly differentially expressed during differentiation stages were used for further analysis. Log_{10}(FPKM+1) RNaseq and LFQ protein data were separately z-score transformed, and WGCNA was performed with a soft-power of 12 signed network. Modules were defined by dynamic tree cut with a minimum module size of 20 (Langfelder and Horvath, 2008). In total 12 modules were identified, ranging in size from 23 to 1119 transcript-protein pairs.

Gene ontology term and WikiPathway (Slenter et al., 2018) enrichment was performed using clusterProfiler (Yu et al., 2012). Manual database annotation were based on Cluster of differentiation, GPCR, FDA approved targets, Transcription factors, Ribosomal proteins: Human protein atlas version 18.1 (Thul et al., 2017); Granule proteins (Rørvig et al., 2013), Meta Adhesome (Horton et al., 2015), Primary immunodeficiency genes (Picard et al., 2015), RNA binding proteins (Gerstberger et al., 2014), RECON1 (Duarte et al., 2007), and MitoCarta 2.0 (Calvo et al., 2016). Enrichment was determined with fisher exact tests followed by Benjamini-Hochberg multiple testing correction.

DATA AND CODE AVAILABILITY

The identifier for .raw MS files and search/identification files obtained with MaxQuant that have been deposited in the ProteomeXchange consortium via the PRIDE partner repository is PRIDE:PXD013785.